Hindawi
Advances in Mathematical Physics
Volume 2024, Article ID 9363431, 22 pages
https://doi.org/10.1155/2024/9363431

*Research Article*

# Analysis of the Dynamics of a Cubic Nonlinear Five-Dimensional Memristive Chaotic System and the Study of Reduced-Dimensional Synchronous Masking

**Lina Ding** and **Pan Wang**

*School of Electronics and Information Engineering, Heilongjiang University of Science and Technology, Harbin 150028, China*

Correspondence should be addressed to Lina Ding; dinglina@usth.edu.cn

Received 4 December 2023; Revised 26 January 2024; Accepted 18 March 2024; Published 26 April 2024

Academic Editor: Zine El Abiddine Fellah



To improve the complexity of the chaotic system and achieve the effective transmission of image information, in this paper, a five-dimensional memristive chaotic system with cubic nonlinear terms is constructed, which has four pairs of symmetric coordinates. First, the cubic nonlinear memristive chaotic system is analyzed using the Lyapunov exponential map, bifurcation map, and attractor phase diagram. The experimental results show that under four pairs of symmetric coordinates, the system exists not only parameter-dependent symmetric rotational coexisting attractor and transient chaotic phenomena but also exists super-multistationary with alternating chaotic cycles dependent on the initial value of the memristor. Then, it is proposed to add a constant term to the linear state variable to explore the effect of the offset increment of the linear state variable on the system in four pairs of symmetric coordinates, while circuit simulation of the five-dimensional chaotic system is carried out using Simulink to verify its existence and realisability. Finally, the synchronization of the dimensionality reduction system and the confidential transmission of the image are achieved, using the control voltage of the system to replace the internal state variables of the memristor to achieve the one-dimensional reduction process, and an adaptive synchronization controller is designed to synchronize the system before and after the dimensionality reduction. Based on the above, an image to be transmitted is modulated into a one-dimensional array and then subjected to the fractional and cyclic operations and combined with the linear encryption and decryption functions and the chaotic masking technique, the simple encryption and decryption of the image processes are realized.

## 1. Introduction

Currently, constructed low-dimensional chaotic systems have problems such as simple structure and low randomness of sequences, but increasing the system dimension can solve these problems; many researchers and scholars have begun to study complex and can produce more random sequences of high-dimensional chaotic systems [1]. Through mathematical models, simulation experiments, and physical experiments, the dynamical properties and behavioral laws of high-dimensional chaotic systems are explored, focusing on the rich dynamical properties of the systems, such as singular attractors, multistability phenomena, and periodical solutions [2, 3], revealing the nonlinear coupling and interaction effects existing in the systems and realizing the control and synchronization of the high-dimensional chaotic systems by designing suitable control methods and coupling modes, which is of great significance for the fields of information processing, data transmission and confidential communication [4–10].

In recent years, chaotic systems and memristors are still in their infancy within the engineering field [11], whereas conventional chaotic systems suffer from the disadvantages of easy deciphering, simple structure, and poor pseudo-randomness of chaotic sequences, the application of memristors to chaotic systems can enhance the complexity of the chaotic systems and extend their dynamics, then enhance the synchronization control and realize the storage functions [12, 13]. More literature exists to study chaotic systems in five or higher dimensions, but there are few studies on constructing high-dimensional chaotic systems based on memristor [14]. Xingze and Junxiu [15] constructed a novel five-dimensional hyperchaotic system with multiple attractors

coexisting in the system by adding a magnetically controlled memristor onto a Lorentzian system, confirming the rich dynamical behaviors of the constructed system. Xiaoxia et al. [16] introduced a magnetically controlled memristor and an absolute value function into a four-dimensional chaotic system to bring the system to a new polarity equilibrium and constructed a conditionally symmetric memristor hyperchaotic system, which systematically generated an infinite number of pairs of coexisting attractors with opposite polarities and similar attractor structures. Ramamoorthy et al. [17] proposed a novel four-dimensional Sprott B recollective chaotic system with a deviation term that switched between rotationally symmetric and nonrotationally symmetric states and has different dynamical behaviors in the two states. Leutcho et al. [18] constructed a new four-dimensional hyperchaotic Lorenz system with heterogeneous multistability phenomena in the new system using a nonlinear feedback controller and verified the experimental results using a digital signal processing platform. Lai et al. [19] and Lai and Chen [20] took the memristor as synapses in a Hopfield neural network, and three memristive Hopfield neural networks were constructed, which could generate multidouble-scroll chaotic attractors or grid multidouble-scroll chaotic attractors and the number of double scrolls in the attractors could be controlled by the memristor. Then, the innovative introduction of two memristors was followed by the construction of an equilibrium-free five-dimensional chaotic system with lattice vortex attractors. In 2023, Lai et al. [21] proposed a framework for constructing super-enhanced memory hyperchaotic maps with four cubic attractors, which improved the complexity of the original maps and effectively solved the discontinuous chaotic range and low Lyapunov exponent problems of common hyperchaotic systems. Xu et al. [22] introduced memristor nonlinear terms and state feedback controllers into a three-dimensional autonomous quadratic class Lorenz chaotic system and constructed a new fourth-order chaotic system, which exhibited rich attractor coexistence. In summary, it is extremely important to construct chaotic systems with rich dynamics by using a memristor.

Chaos synchronization refers to the phenomenon that there exists some kinds of coupling mechanism between two or more chaotic systems so that their states tend to agree with each other in time and chaos synchronization has important applications in the fields of communication, secure transmission, and information processing [23–27]. At present, the researches on synchronous control of low-dimensional chaotic systems are more comprehensive, while the theoretical researches on synchronous control of high-dimensional chaos are under development, especially the researches on the realization of synchronization of chaotic systems of different dimensions are still scarce. Emiroglu et al. [28] studied the problem of control of chaos in a ferroresonant circuit using backstepping nonlinear control to become stable in the equilibrium point and converge to the desired trajectory or point and demonstrated the effectiveness of designed control inputs for chaos control in ferroresonant phenomena. Then, Emiroglu et al. [29] proposed a passive synchronization control method based on the new four-dimensional chaotic system to achieve the synchronization of the new four-dimensional chaotic system hyperchaotic system with different initial conditions. Alexander et al. [30] designed a controller based on linear quadratic regulatory control and applied it to nonautonomous systems with infinite coexisting attractors, and the effectiveness of the controller was demonstrated through error. Chi [31] designed a proper synchronous controller using active synchronous control methods to study the synchronous control of two different dimensional memristor hyperchaotic systems and proved the controller using the Routh Criterion theorem. Liu [32] combined the designed five-dimensional memristor hyperchaotic system with a chaotic system of the same number of dimensions to achieve the synchronization of heterostructured chaotic systems based on active control. Shi [33] used the nonlinear feedback synchronization and linear feedback synchronization control method to achieve the synchronization of two 3D (three-dimensional) chaotic systems and carried out circuit simulation using Multisim software, and the experimental results were consistent with the numerical analyses, thus verifying the feasibility of the synchronization control of the new 3D chaotic circuits. In summary, synchronous control of chaotic systems is extremely important to study [34–37].

Although the introduction of memristor into chaotic systems has been reported in the literature, few studies guarantee the inclusion of both memristor and the presence of only cubic nonlinear terms in high-dimensional chaotic systems, especially since the dynamical phenomena with which the system are endowed will be reduced while increasing the dimensionality and complexity of the system. Therefore, in this paper, a five-dimensional chaotic system is constructed contains both a memristor and a nonlinear term that occurs only three times to ensure that it has a rich dynamical behavior as well as that the sequences it produces can be applied in the field of image encryption. In terms of achieving synchronization, the techniques for achieving synchronization of low-dimensional chaotic systems are maturing, but there are few reports in the literature on the synchronization of high-dimensional chaotic systems with their downscaled systems themselves, so in this paper, the synchronization control of downscaled systems is investigated. First, the magnetically controlled memristor is introduced, which is based on the Liu pseudo-four-wing three-dimensional chaotic system proposed by Bocheng et al. [38]. It is improved to a five-dimensional system with three nonlinear terms by adding two equations and multiplying all the quadratic nonlinear terms in the equations by the state variable $x$ in the system, which has four pairs of symmetric coordinates. The attractor phase diagrams, time domain waveforms, etc., are simulated by MATLAB 2018a and the fractional dimension is calculated by combining with the wolf algorithm to prove that the constructed system is a chaotic system. Second, it is verified that the attractors generated by the system in all four pairs of symmetric coordinates have rotationally symmetric properties when the coupling parameter and the initial value are used as controllable variables in turn, as well as that the system has a rich dynamical behavior. There are not only parameter-dependent periodic, chaotic symmetric rotational attractors and transient chaotic phenomena but

also super-multistationary phenomena with alternating chaotic cycles that depend on the initial value of the memristor. The effect of linear state variable offset increments on the system is then explored and Simulink circuit simulation is used to verify the correctness of the system. Finally, the important dynamics of the system are retained, the five-dimensional chaotic system is downgraded, the system is synchronously controlled before and after the downgrading using the adaptive synchronous control method, and the encryption and decryption of the image are realized by combining the chaos masking technique and the encryption and decryption functions. There are also super-multistable phenomena with alternating chaotic cycles that depend on the initial value of the memristor.

## 2. Construction of a Cubic Nonlinear Five-Dimensional Memristor System

*2.1. System Model.* Professor Bocheng et al. [38] proposed a smooth magnetically controlled memristor model in 2010, which had the characteristics of a relatively simple mathematical model and was easy to make the system produce complex, chaotic signals, etc. The model has been widely used by scholars in chaotic systems to construct new memristive chaotic systems. The memristor model is expressed as follows:

$$\begin{cases} i = W(\phi)v \\ W(\phi) = m + n\phi^2 \\ \dot{\phi} = v \end{cases}, \tag{1}$$

where $W(\phi)$ is the memristor function, $m$ and $n$ are both positive constants. $i$ and $v$ denote the terminal current and terminal voltage flowing through the memristor. $\phi$ denotes the internal flux of the memristor.

In 2003, Liu [39, 40] proposed a pseudo quadruple chaotic system, which belonged to the generalized Lorenz system, and its mathematical expression is shown in Equation (2):

$$\begin{cases} \dot{x} = ax - byz \\ \dot{y} = -cy + xz \\ \dot{z} = -dz + xy \end{cases}, \tag{2}$$

where $x, y$, and $z$ are the three state variables of the system (2). $a, b, c$, and $d$ are the system parameters.

In order to study the effects of the dynamical behavior of a five-dimensional chaotic system containing a memristor with a cubic nonlinear term, based on the system (2), adding two new equations: the fourth equation and the fifth equation. Introducing the memristor in Equation (1) into the fourth equation and choosing the control voltage $y$ as the fifth equation, all the nonlinear terms in the equations are multiplied by $x$, so that all the nonlinear terms in the first, second and third equations are transformed into a five-dimensional system of cubic nonlinear terms, a new five-dimensional memristor hyperchaotic system is constructed. This chaotic system contains a memristor, six linear terms, and three cubic nonlinear terms, which are mathematically modeled as follows:

$$\begin{cases} \dot{x} = ax - xyz \\ \dot{y} = by + x^2 z - cw \\ \dot{z} = x^2 y - dz \\ \dot{w} = kW(u)y - w \\ \dot{u} = ey \end{cases}, \tag{3}$$

where $x, y, z, w$, and $u$ are the five state variables of system (3). $a, b, c, d, e$, and $k$ are the system parameters.

*2.2. Validation of the Five-Dimensional Memristor System.* This article analyzes the Lyapunov exponent diagram, bifurcation diagram, time-domain waveform diagram, and attractor phase diagram simulated in MATLAB 2018a to identify whether the characteristics and behavior of the system are consistent with the ideal phenomenon. Through sufficient theoretical analysis and experimental exploration, continuous parameter verification and adjustment are carried out, and the initial parameters and conditions of the system are preliminarily determined. Let $a = 3, b = -8, c = 3, d = 5, e = 1, k = 40, m = 1$, and $n = 0.01$. The initial condition is $(1; -1; -10; 1; -10)$. Numerical simulation is carried out using the fourth-order Runge-Kutta method and the attractor phase diagrams in the $x-y, x-z, x-w, y-z, y-w$, and $z-w$ planes are shown in Figure 1. It can be simply and intuitively observed that the system behaves irregularly, and therefore, the system (3) is ergodic.

The corresponding five Lyapunov exponents are $\mathrm{LE}_1 = 1.24, \mathrm{LE}_2 = 0.001373, \mathrm{LE}_3 = -0.03694, \mathrm{LE}_4 = -4.812$ and $\mathrm{LE}_5 = -10.39$. The dimension of the Lyapunov exponent computed by Wolf's algorithm is shown as follows:

$$D_L = j + \frac{1}{\left|\mathrm{LE}_{j+1}\right|}\sum_{i=1}^{j}\mathrm{LE}_i = 3 + \frac{\mathrm{LE}_1 + \mathrm{LE}_2 + \mathrm{LE}_3}{\left|\mathrm{LE}_4\right|} = 3.250. \tag{4}$$

The 0–1 test plot of the system (3) in the plane of $y-u$ is shown in Figure 2(a), and the time domain waveforms of the system in $x-t, y-t, z-t, w-t$, and $u-t$ planes are shown in Figure 2(b). The system is chaotic because the Lyapunov exponential dimension $D_L$ is fractional dimensional, the 0–1 test chart is Brownian motion, and the time domain waveform is nonperiodic.

## 3. Basic Dynamic Properties

*3.1. Symmetry.* The newly constructed system has four symmetrical coordinates $(x, y, z, w, u), (x, -y, -z, -w, -u)$, $(-x, y, z, w, u)$, and $(-x, -y, -z, -w, -u)$.

*3.2. Dissipative.* The dissipation of system (3) can be expressed as follows:

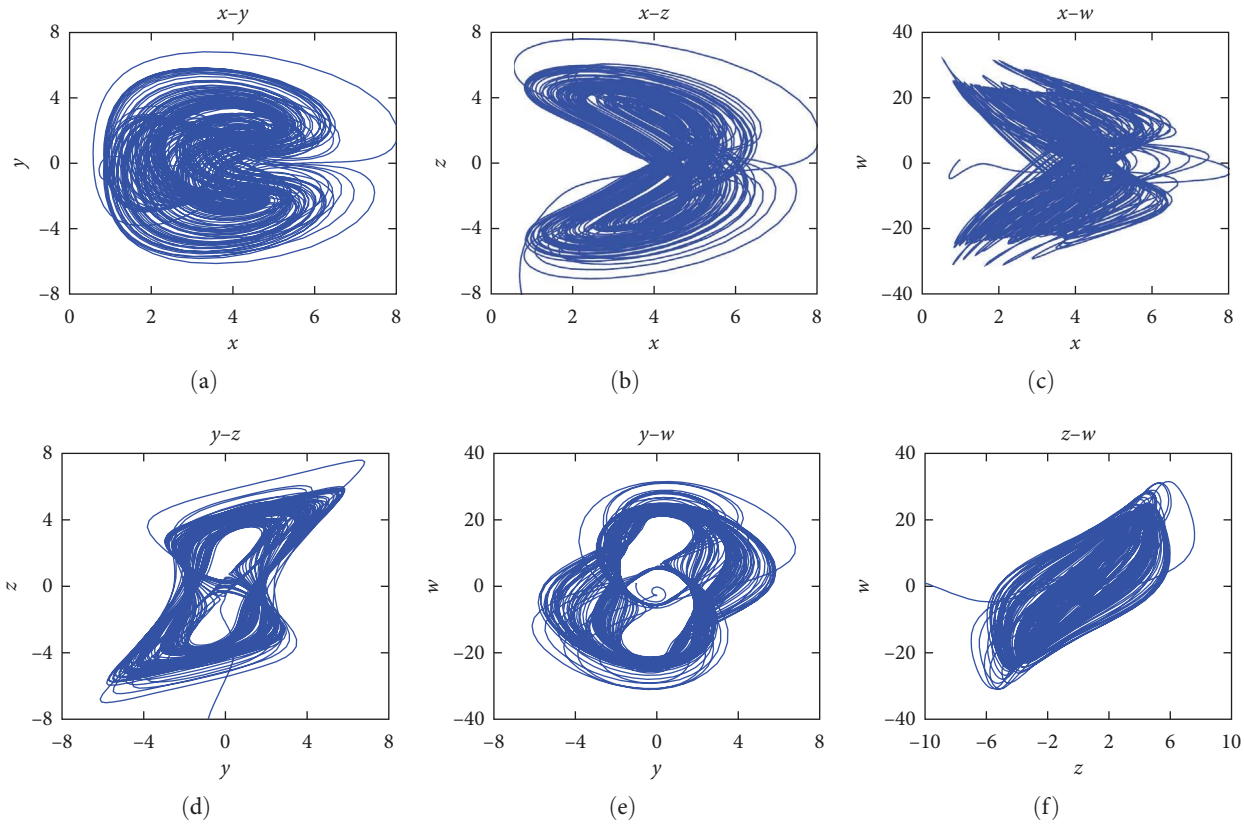


FIGURE 1: Basic phase diagrams of the system: (a) the $x-y$ plane; (b) the $x-z$ plane; (c) the $x-w$ plane; (d) the $y-z$ plane; (e) the $y-w$ plane; (f) the $z-w$ plane.

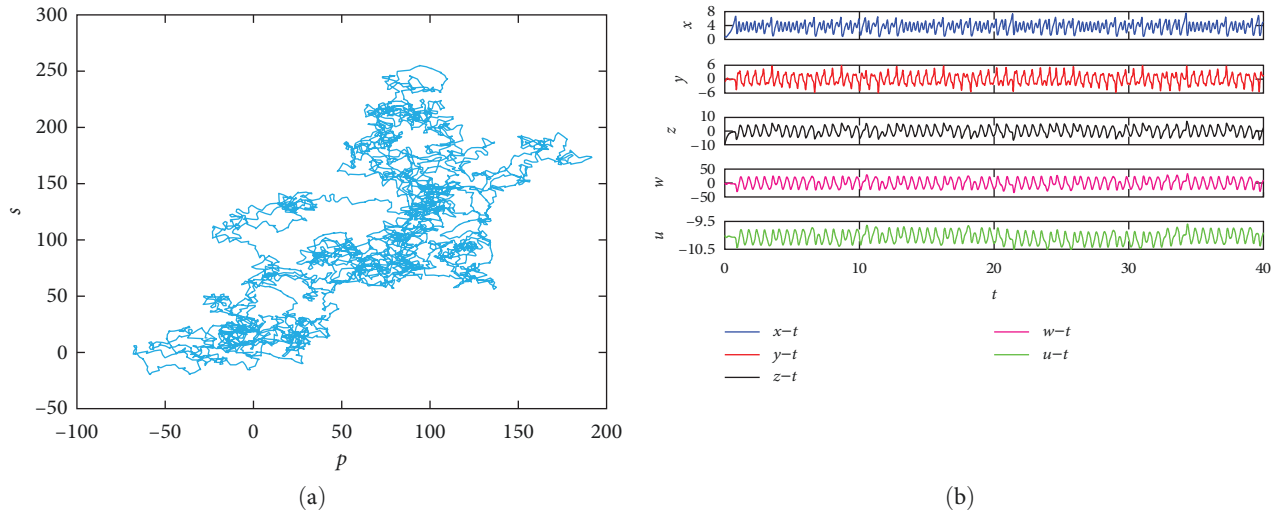


FIGURE 2: 0–1 test plot and time domain waveforms with parameters $a=3, b=-8, c=3, d=5, e=1, k=40, m=1$, and $n=0.01$: (a) 0–1 test plot; (b) time-domain waveforms.

$$\nabla v = \frac{\partial \dot{x}}{\partial x} + \frac{\partial \dot{y}}{\partial y} + \frac{\partial \dot{z}}{\partial z} + \frac{\partial \dot{w}}{\partial w} + \frac{\partial \dot{u}}{\partial u} = a - yz + b - d - 1. \quad (5)$$

When $a=3, b=-8$, and $d=5$, then $\nabla v = -11 - yz$, when $yz>0$, whatever the values of the other parameters of the system are, it does not affect the value of the dissipation degree $\nabla v$. At this point, the system (3) is dissipative when $t$ tends to infinity, the system converges over time in an exponential form $dV/dt = e^{-11-yz}$ and ultimately all the trajectories contract in a subset of volume 0 and attach to an

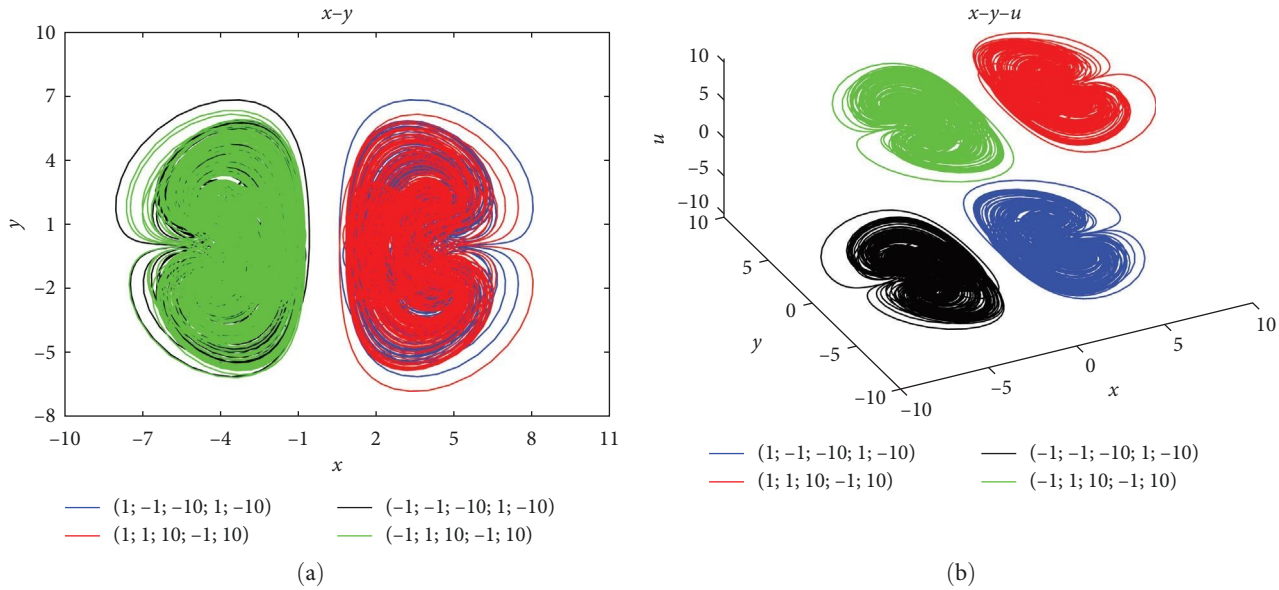


FIGURE 3: Phase space diagrams: (a) the 2D (two-dimensional) planar attractor phase diagram; (b) the 3D planar attractor phase diagram.

attractor. When $yz < -11$, the system (3) has conservatism, and ultimately, its trajectories will no longer be adsorbed on the attractor.

*3.3. Equilibrium Stability.* Let $\dot{x} = \dot{y} = \dot{z} = \dot{w} = \dot{u} = 0$, the equilibrium point of the system (3) be obtained as $-S(0, 0, 0, 0, \eta)$. $\eta$ is an arbitrary real constant, there are infinitely many equilibrium points of the system and the Jacobi matrix at the equilibrium point $-S(0, 0, 0, 0, \eta)$ is as follows:

$$J_s = \begin{bmatrix} a & 0 & 0 & 0 & 0 \\ 0 & \mathrm{b} & 0 & -c & 0 \\ 0 & 0 & -d & 0 & 0 \\ 0 & kW(\eta) & 0 & -1 & 0 \\ 0 & e & 0 & 0 & 0 \end{bmatrix}. \tag{6}$$

The characteristic polynomial at the equilibrium point $-S(0, 0, 0, 0, \eta)$ is as follows:

$$P(\lambda) = \lambda(\lambda^4 + p_1\lambda^3 + p_2\lambda^2 + p_3\lambda + + p_4) = 0. \tag{7}$$

The coefficients of the quadratic polynomial are as follows:

$$\begin{cases} p_1 = \mathrm{d} - \mathrm{b} - a + 1 \\ p_2 = (a - d)(b - 1) - \mathrm{ad} - b + ckW(\eta) \\ p_3 = (b - ckW(\eta))(a - d) + ad(b - 1) \\ p_4 = ad(b - ckW(\eta)) \end{cases}. \tag{8}$$

The computation of Equation (7) yields that the characteristic polynomial has one zero and four nonzero characteristic roots. For the nonzero characteristic roots, the Routh–Hurwitz stability conditions for the quadratic polynomial are as follows:

$$\begin{cases} \Delta_1 = p_1 > 0, p_4 > 0 \\ \Delta_2 = p_1 p_2 - p_3 > 0 \\ \Delta_3 = p_1(p_2 p_3 - p_1 p_4) - p_3^2 > 0 \end{cases}. \tag{9}$$

When all three conditions of Equation (9) are satisfied simultaneously, the equilibrium point is stable, and the system produces point attractors; when any of the conditions in Equation (9) is not satisfied, the equilibrium point is unstable, and the system behaves as a periodic or chaotic state. The calculation shows that $p_4 > 0$ in Equation (9) is always unsatisfied, so the system always behaves in a chaotic or periodic state. The line equilibrium point on the $u$-axis at the time of the system, according to the Jacobi matrix polynomials, the eigenvalues $\lambda_1 = 0, \lambda_2 = -5, \lambda_3 = 3, \lambda_4 = (24a^2/5 + 431)^{1/4} - 4.5$, and $\lambda_5 = (-24a^2/5 - 431)^{1/4} - 4.5$ whose eigenroots are not all positive or negative, so that there are countless unstable saddle points on the line equilibrium point, which implies that the attractor is hidden [41].

## 4. Dynamic Analysis of the System in Symmetric Coordinates

Since the system has four symmetric coordinates: $(x, y, z, w, u), (x, -y, -z, -w, -u), (-x, y, z, w, u)$, and $(-x, -y, -z, -w, -u)$. In this paper, select the corresponding four initial values of the coordinates which are $(1, -1, -10, 1, -10), (1, 1, 10, -1, 10), (-1, -1, -10, 1, -10)$, and $(-1, 1, 10, -1, 10)$. The attractor phase diagrams are obtained, as shown in Figure 3, in which the initial value of the blue track line is $(1, -1, -10, 1, -10)$, the initial value of the red track line is $(1, 1, 10, -1, 10)$, the initial value of the black track line is $(-1, -1, -10, 1, -10)$ and the initial value of the green track line is $(-1, 1, 10, -1, 10)$. When four

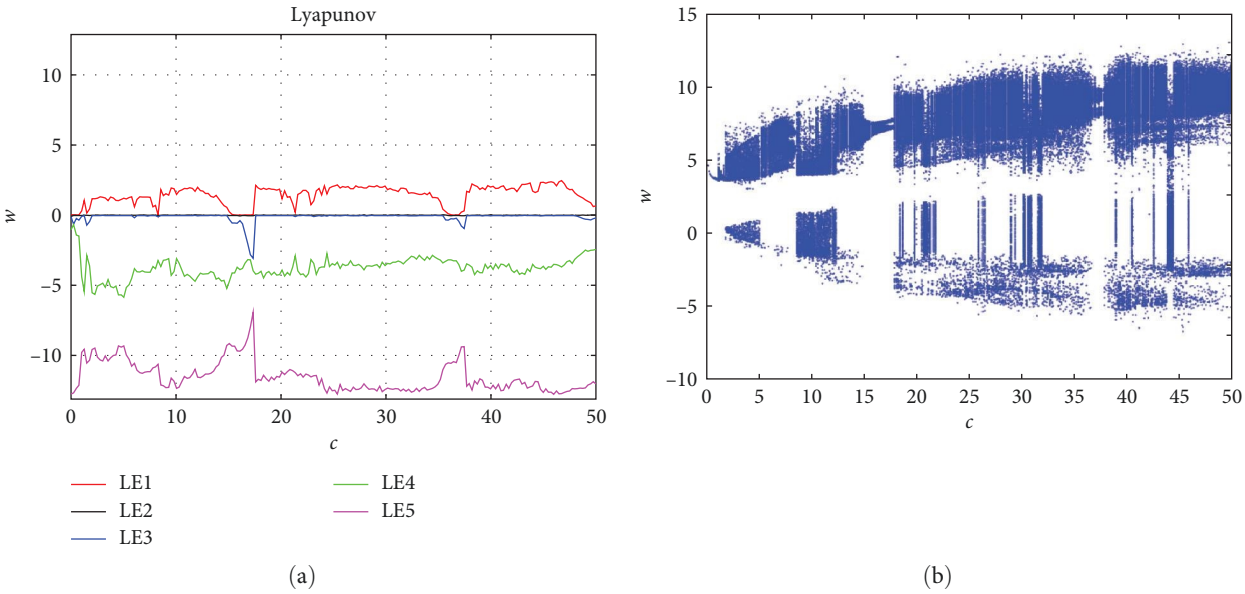


Figure 4: Bifurcation diagram and Lyapunov exponent spectrum of chaotic system with $c \in [0, 50]$: (a) the Lyapunov exponential spectra; (b) the bifurcation diagram.

symmetrically different initial values are taken, the attractors take on the state of a symmetrically rotated attractor, and each attractor undergoes a rotational translation transformation to obtain the remaining three attractors. To explore the crossing of the four rail lines, the three-dimensional attractor phase diagram of the $x - y - u$ plane is plotted, as shown in Figure 3(b). It can be observed that the four rail lines are independent of each other and do not cross each other, and thus, the system can generate identical symmetric rotating coexisting attractors at different initial values. Therefore, all the studies in this paper are based on these four pairs of symmetric coordinates to investigate the rich dynamical behaviors of the system depending on the coupling parameters and initial values of the system.

*4.1. Parameter-Dependent Symmetric Rotational Attractors and Transient Chaotic Phenomena.* Let the system parameter $c$ be a variable control parameter and the fixed parameters $a = 3$, $b = -8$, $c = 3$, $d = 5$, $e = 1$, $k = 40$, $m = 1$, and $n = 0.01$. The Lyapunov exponential diagram of the system state variable $w$ varying in the parameter $c \in [0, 50]$ is shown in Figure 4(a) and the bifurcation diagram is shown in Figure 4(b). As can be seen from Figure 4, the Lyapunov exponential diagram is consistent with the bifurcation diagram, and the system has one positive and two positive Lyapunov exponential values alternating in the interval, so the system has rich dynamics, alternating between cyclic and chaotic states and the parameter $c$ has a greater range of adjustability and unpredictability and the resulting sequences will be more stochastic.

When parameter $c = 0.18$, the corresponding first Lyapunov exponential spectrum is tangent to the zero line and the corresponding five Lyapunov exponents are 0.02367, $-0.03143$, $-0.05826$, $-0.6184$, and $-12.78$, one of which is approaching zero and the remaining four exponents are less than zero and it can be judged that the system is running in a periodic orbit at this time and the system is in a periodic three-attractor coexistence state under all four symmetric coordinate systems, as shown in Figure 5(a); when parameter $c = 0.7538$, the system has a positive Lyapunov exponent value close to 0 and the system is in a periodic four-attractor coexistence state under the four symmetric coordinates, as shown in Figure 5(b); when the parameter $c = 1.05$, the system has a positive Lyapunov exponent value and the system is in a periodic five-attractor coexistence state under the four symmetric coordinates, as shown in Figure 5(c); when the parameter $c = 2.6$, the system has two positive Lyapunov exponent values and the system is in a chaotic coexistence state under the four symmetric coordinates, as shown in Figure 5(d). Where the blue color indicates the initial value of $(1, -1, -10, 1, -10)$, the red color indicates the initial value of $(1, 1, 10, -1, 10)$, the black color indicates the initial value of $(-1, -1, -10, 1, -10)$ and the green color indicates the initial value of $(-1, 1, 10, -1, 10)$. From Figure 5, it can be seen that the system exists the same symmetric rotationally coexisting attractor phenomenon under different values of the parameter $c$.

To observe the periodic, chaotic alternating state of the chaotic system more clearly, a larger time interval is chosen, and the state of the system is analyzed by combining the time-domain waveforms with four pairs of symmetric coordinates corresponding to $x - t$. When $c = 15.8$, the system is in a periodic state, and the attractor phase diagram and time-domain waveforms are shown in Figure 6(a); when $c = 25$, the system is in a chaotic state, and the attractor phase diagram and time-domain waveforms are shown in Figure 6(b); when $c = 36.47$, the system is in a periodic state and the attractor phase diagram and time domain waveform are shown in Figure 6(c); when $c = 42$, the system is in a chaotic state and the attractor phase diagram and time domain waveform are shown in Figure 6(d). So, the system has a rich dynamical behavior.

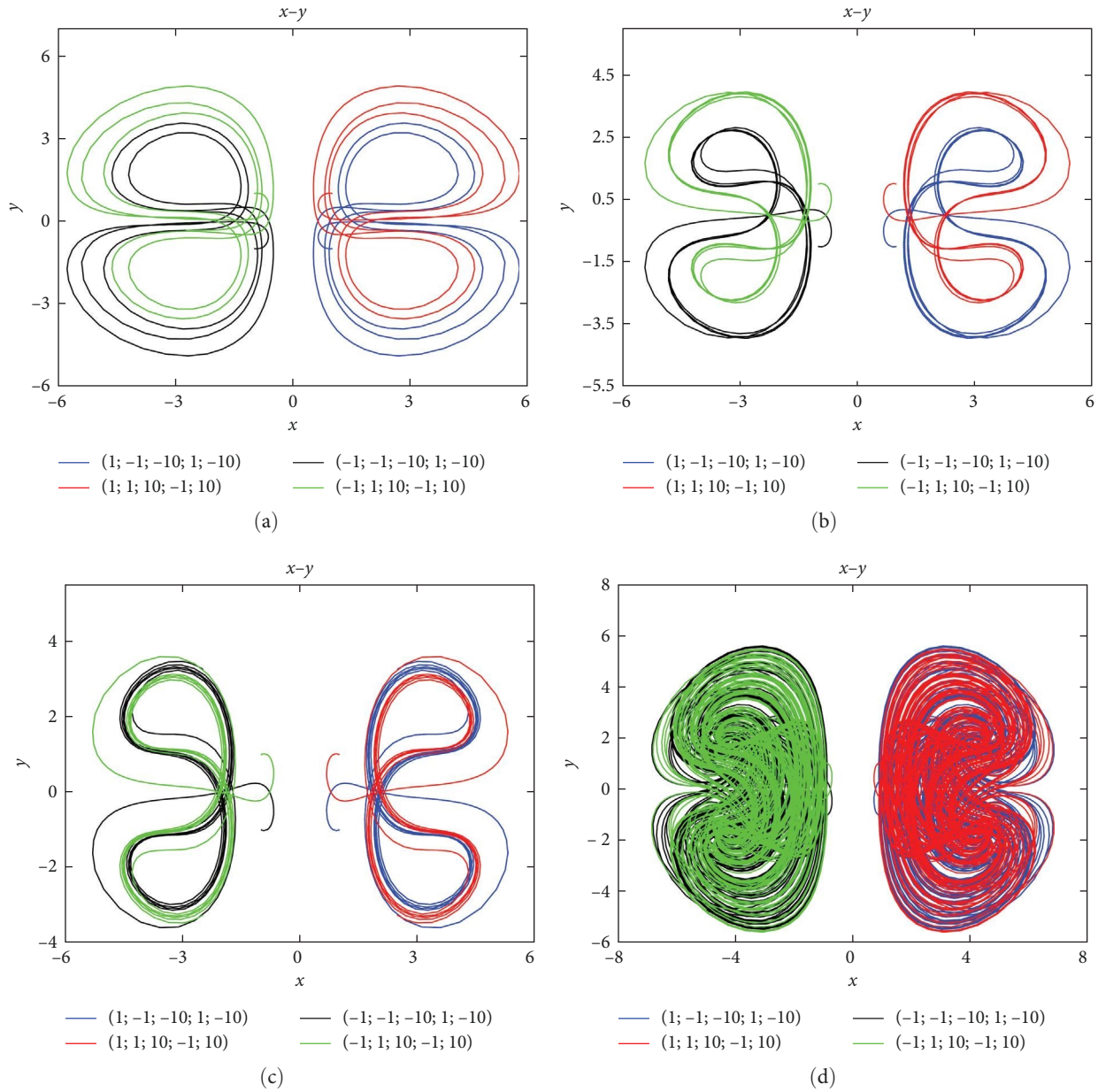


Figure 5: Various attractor phase diagrams varying with $c$: (a) $c = 0.18$; (b) $c = 0.7538$; (c) $c = 1.05$; (d) $c = 2.6$.

By observing the time-domain waveform graph of Figure 6(a) at time $c = 15.8$, it can be seen that the system is in a chaotic state at $t \in [0, 15]$ and a cyclic state at $t \in [15, 50]$. This phenomenon is referred to as transient chaos [32], which is due to the presence of non-attractive saddle points, resulting in the system appearing chaotic for a finite period and then transforming into nonchaos after some time change. The attractor phase diagram about the $x - y$ plane in the $t \in [0, 15]$ time interval is shown in Figure 7(a) and the attractor phase diagram about the $x - y$ plane in the $t \in [15, 50]$ time interval is shown in Figure 7(b).

*4.2. Super Multistability Phenomena Dependent on the Initial Value of Memristor Resistance.* Chaotic systems have strong initial value sensitivity; small differences in initial conditions will cause significant differences in the evolution of the system [42, 43], which ultimately leads to the separation of the trajectory of the system, even if the initial conditions of the two systems are very close to each other, the results of their evolution may also be extremely different. Choose two initial values as $(1, -1, -10, 1, -10)$ and $(1, -1, -10, 1, -10.001)$, respectively, and both of them are different by 0.001 in the initial value of $u0$. The time domain waveform graphs and attractor phase diagrams for the two initial values are simulated as shown in Figures 8(a) and 8(b), in which the blue waveform initial value is $(1, -1, -10, 1, -10)$ and the red waveform initial value is $(1, -1, -10, 1, -10.001)$. It shows large differences in the time domain waveform diagrams when the initial value is changed by 0.001, the time domain waveforms change approximately regularly, the trajectory of the

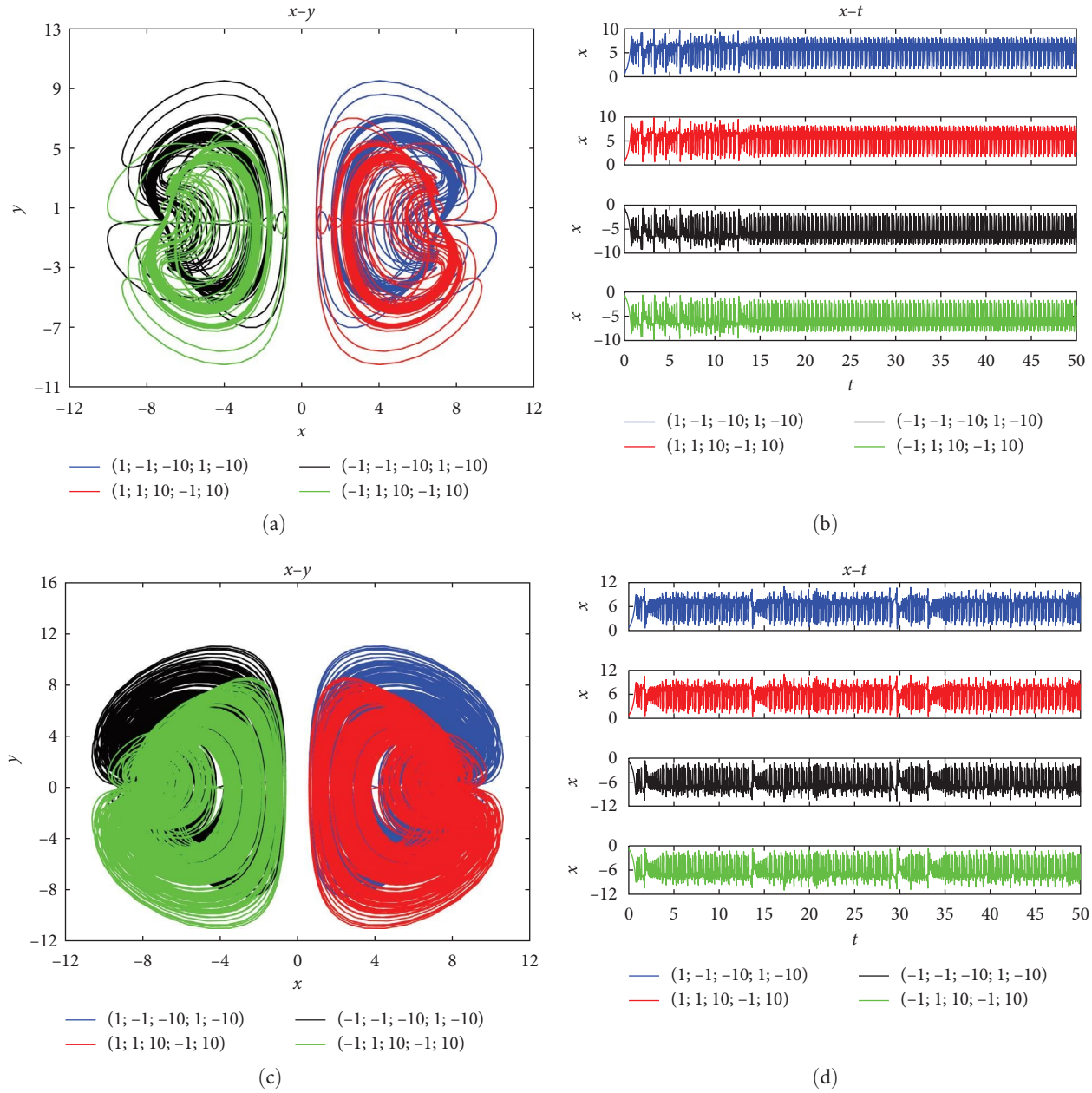


Figure 6: Continued.

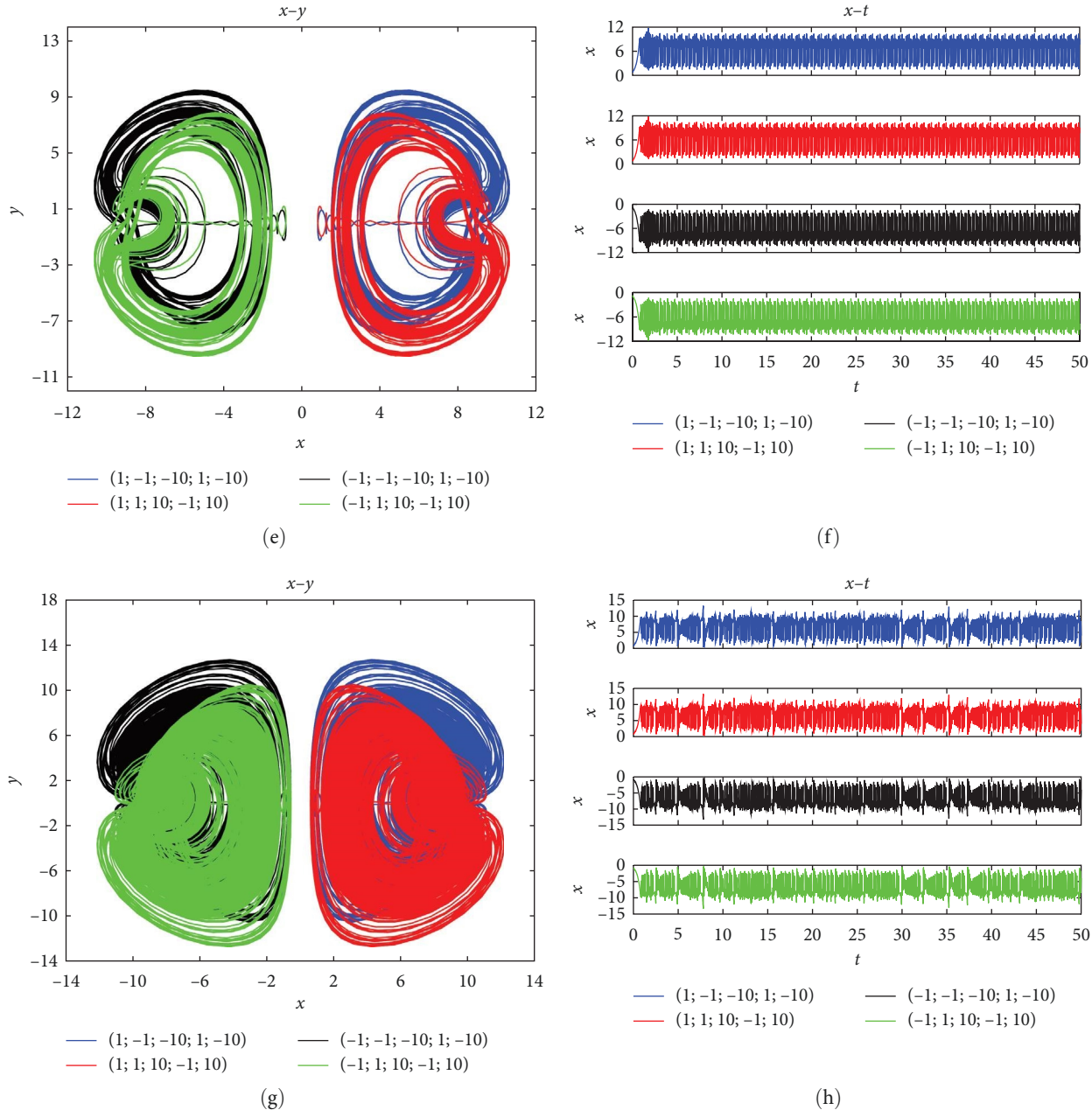


FIGURE 6: Various attractor phase diagrams varying and time-domain waveforms with $c$: (a) attractor phase diagram with parameter $c = 15.8$; (b) time-domain waveform with parameter $c = 15.8$; (c) attractor phase diagram with parameter $c = 25$; (d) time-domain waveform with parameter $c = 25$; (e) attractor phase diagram with parameter $c = 36.47$; (f) time-domain waveform with parameter $c = 36.47$; (g) attractor phase diagram with parameter $c = 42$; (h) time-domain waveform with parameter $c = 42$.

initial value of $(1, -1, -10, 1, -10)$ is always follows the change of $(1, -1, -10, 1, -10.001)$ and the trajectory of attraction subphase diagrams shows two symmetrical states and the system has a stronger sensitivity to the initial value.

Thanks to the initial value sensitivity of $u0$, the fixed system parameters, the initial value of memristor $u0$ is chosen as a variable parameter, the other initial values are $x0 = 1$, $y0 = -1, z0 = -10, w0 = 1$ and the fixed parameters $a = 3, b = -8, c = 3, d = 5, e = 1, k = 40, m = 1,$ and $n = 0.01$. The Lyapunov exponent of the state variable $z$ for the memristor initial value condition $u0 \in [0, 30]$ is plotted as shown in Figure 9(a) and the bifurcation diagrams are shown in Figure 9(b). From Figure 9, it can be seen that the system has a rich dynamical behavior, transforming in two states: chaotic and periodic.

The super multistability property is a complex nonlinear phenomenon in chaotic systems, which refers to the fact that an infinite number of coexisting attractors with different states of motion can be generated by changing the initial state of the system with fixed system parameters [31]. The multistability phenomenon of the system at different initial values of the memristor is analyzed by fixing the system parameters and

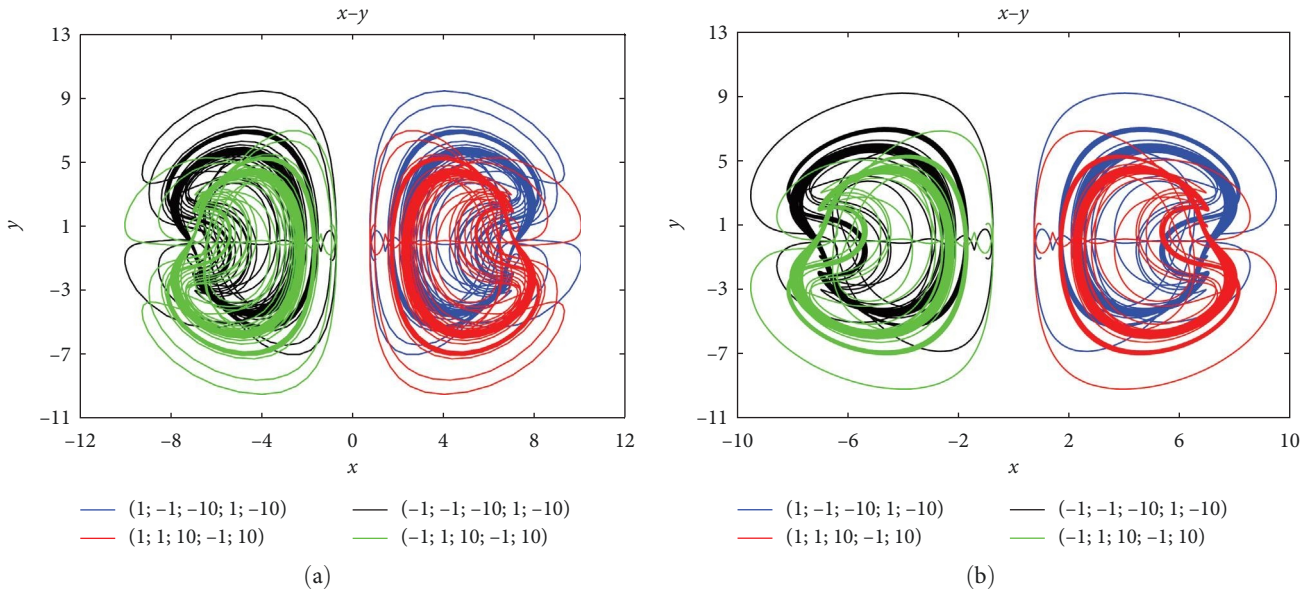


Figure 7: When $c = 15.8$,various phase diagrams varying with $t$: (a) $t \in [0, 15]$; (b) $t \in [15, 50]$.

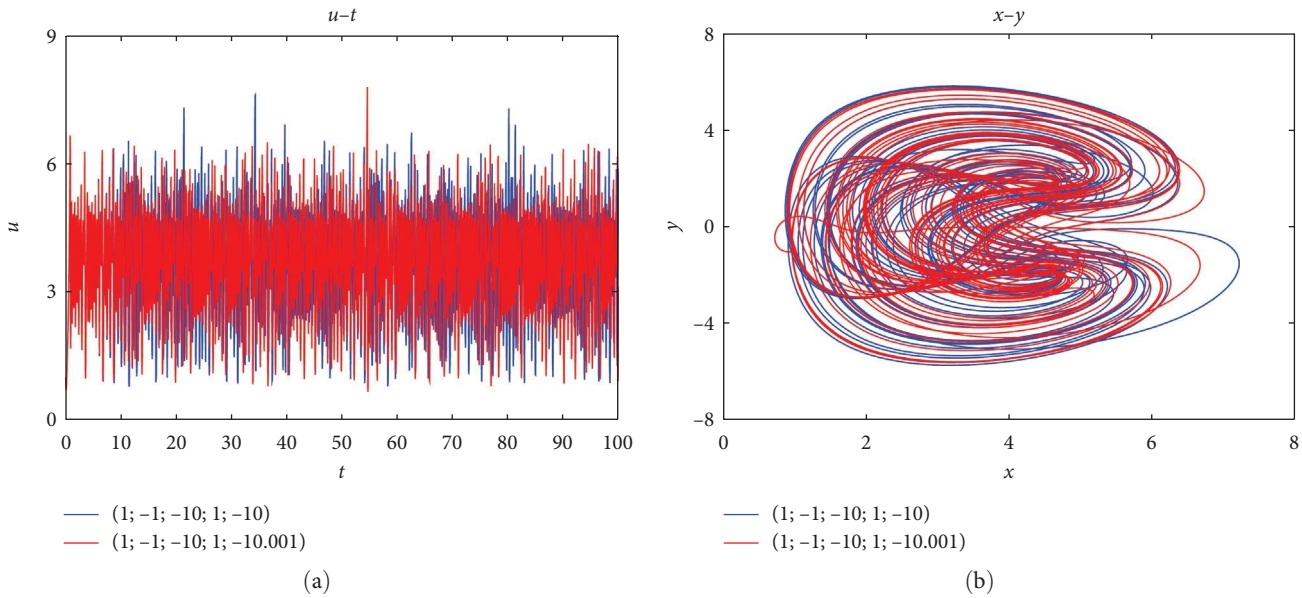


Figure 8: Time domain waveform and attractor phase diagram for initial values of $(1; -1; -10; 1; -10)$ and $(1; -1; -10; 1; -10.001)$: (a) the time-domain waveform; (b) the attractor phase diagram.

combining the phase diagrams of the attractors in four pairs of symmetric coordinates. When $u0 = 5$, the attractor phase diagram under four symmetric coordinates is shown in Figure 10(a); the attractor of the system is in a chaotic state; when $u0 = 21.5$, the attractor phase diagram under four symmetric coordinates is shown in Figure 10(b); the attractor of the system is in a cyclic state; when $u0 = 25$, the attractor phase diagram under four symmetric coordinates is shown in Figure 10(c), the attractor of the system is in a chaotic state; and when $u0 = 30$, the attractor of the system is in a chaotic state. The attractor phase diagram under four symmetric coordinates is shown in Figure 10(d), the attractor of the system is in a periodic state. Where blue indicates that the initial value is $(1, -1, -10, 1, -u0)$, red indicates that the initial value is $(1, 1, 10, -1, u0)$, black indicates that the initial value is $(-1, -1, -10, 1, -u0)$ and green indicates that the initial value is $(-1, 1, 10, -1, u0)$. Therefore, the system has multiple coexisting attractors with repeated alternation of chaotic cycles, and the different state attractors undergo interconversion, which proves that the new system has the phenomenon of super-multistability with repeated alternation of chaotic cycles.

*4.3. Control of Linear State Variable Offset Increments.* In a deterministic nonlinear system, a state variable is predicted to occur only once in that system; the addition of a constant

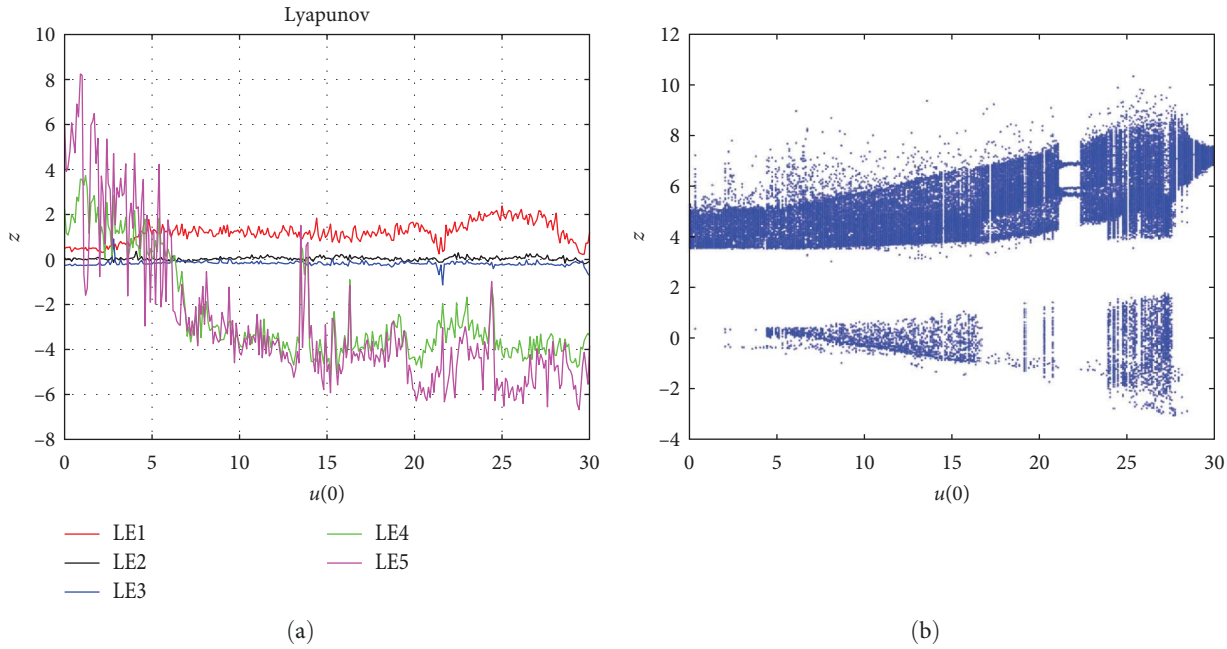


FIGURE 9: Bifurcation diagram and Lyapunov exponent spectrum of chaotic system with $u0 \in [0, 30]$: (a) the Lyapunov exponential spectra; (b) the bifurcation diagram.

term to the state variable will produce a controllable offset that will change the chaotic system from unipolar to bipolar [43]. When a constant is introduced into the variable, the differential equation does not change its form, and the offset increment control allows chaotic signals to be interchanged between bipolar and unipolar without changing the fundamental dynamics of the system, simply by changing an additional control constant [44]. From system (3), it can be seen that the system does not have a state variable that occurs only once on the right-hand side. So, in this paper, it is proposed to add a constant term to the linear state variable to produce a controllable offset to change the chaotic system from unipolar to bipolar. Choosing to add a constant term to the linear variable $y$ in the second equation, using the state variable $y \pm l$ instead of $y$, where $l$ is the offset increment controller, the new equation is as follows:

$$\begin{cases} \dot{x} = ax - yzx \\ \dot{y} = b(\mathrm{y} + l) + x^2 z - cw \\ \dot{z} = x^2 y - dz \\ \dot{w} = kW(u)y - w \\ \dot{u} = ey \end{cases} . \tag{10}$$

Changing the size of $l$ in a certain range, the chaotic attractor can be realized to move on the $x - w$ axis. When $l = 10, l = 0$, and $l = -10$ are selected, the initial condition is $(1, -1, -10, 1, -10)$ and the phase trajectory diagram of the $x - w$ plane is simulated, as shown in Figure 11(a); the initial condition is $(1, 1, 10, -1, 10)$ and the phase trajectory diagram of the $x - w$ plane is simulated, as shown in Figure 11(b); the initial condition is $(-1, -1, -10, 1, -10)$ and the phase trajectory diagram of the $x - w$ plane is simulated, as shown in Figure 11(c); the initial condition is $(-1, 1, 10, -1, 10)$, the phase trajectory of the $x - w$ plane is shown in Figure 11(d). Where blue color indicates the attractor at $l = 0$, black color indicates the attractor at $l = 10$ and red color indicates the attractor at $l = -10$. From Figure 11, it can be seen that for the add operation, the attractor phase trajectory diagrams are all located below $l = 0$ and for the subtract operation, the attractor phase trajectory diagrams are all located above $l = 0$. Therefore, the attractor can realize the single-bipolar transition on the $w$-axis when the linear state variable offset is changed.

## 5. Circuit Simulation

Simulink has the advantages of high visualization, multidomain simulation, fast modeling and iteration, high accuracy, etc. Therefore, in this paper, the Simulink platform is chosen to build circuits for the new five-dimensional chaotic system. The circuit built is shown in Figure 12, the phase diagrams of the attractor obtained by simulation are shown in Figure 13, and the time domain waveform diagrams in the planes are shown in Figure 14. Both the attractor phase diagrams and the time domain waveform diagrams are consistent with the trajectories simulated by MATLAB 2018a numerical analysis, which verifies the correctness of the five-dimensional chaotic system.

## 6. Reduced Dimensional Synchronization and Image Encryption

*6.1. System Downgrading Process.* To realize the synchronous control of a chaotic system before and after dimensional

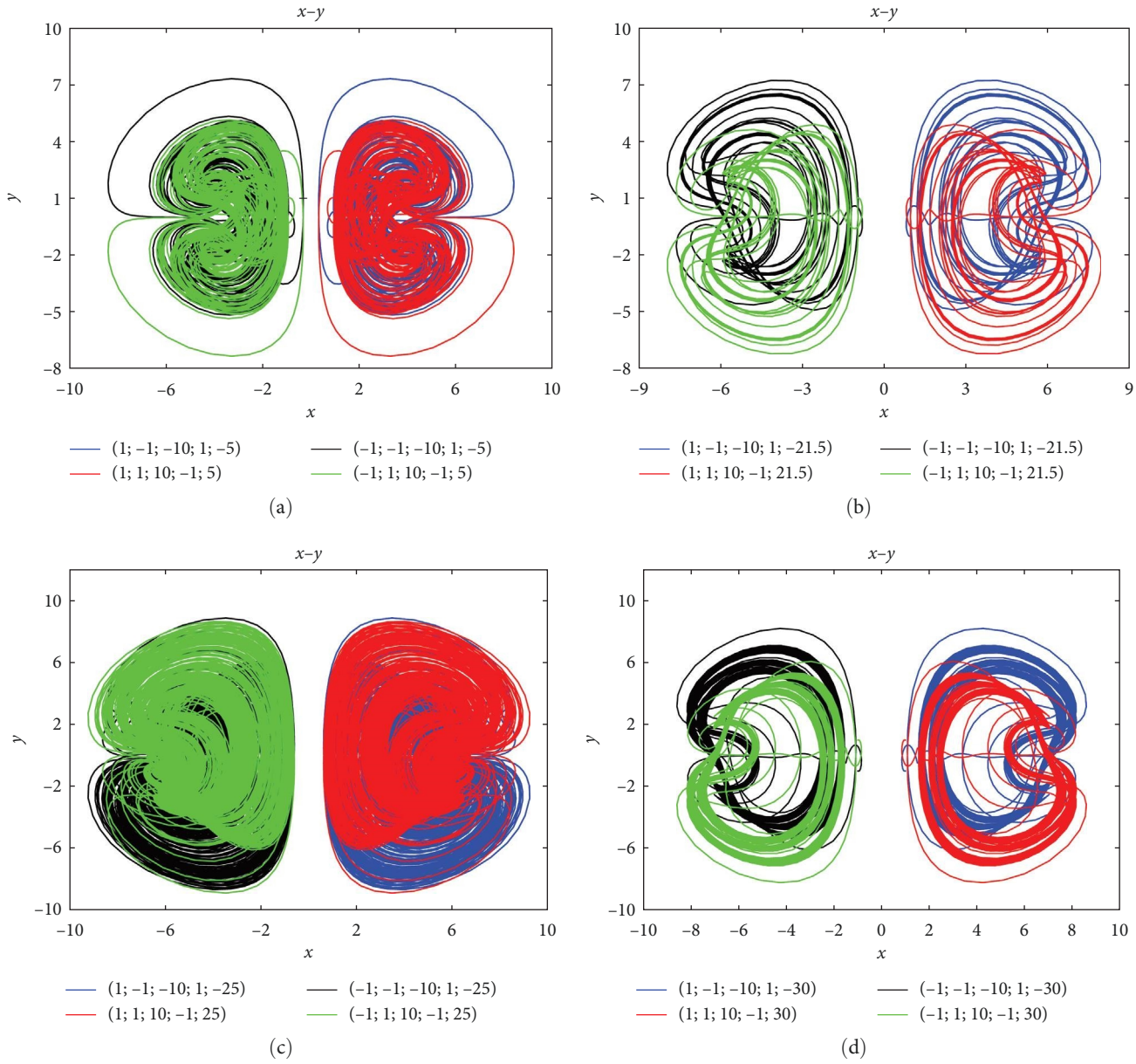


FIGURE 10: Various phase diagrams varying with $u0$: (a) $u0 = 5$; (b) $u0 = 21.5$; (c) $u0 = 25$; (d) $u0 = 30$.

reduction, it is necessary to carry out the dimensional reduction process on the newly constructed system (3), the control voltage in the system equations with the internal state variables of the memristor is replaced, all the parameter $u$ in the equations will be defined as parameter $y$ and the four-dimensional chaotic system after dimensional reduction will be obtained as follows:

$$\begin{cases} \dot{x} = ax - xyz \\ \dot{y} = by + x^2 z - cw \\ \dot{z} = x^2 y - dz \\ \dot{w} = kW(y)y - w \end{cases}. \tag{11}$$

Let $a = 3, b = -8, c = 4, d = 5, e = 1, k = 40, m = 1,$ and $n = 0.01$ and the initial condition be $(1, -1, -10, 1)$. The attractor phase diagrams of the planes of $x - y, x - z, x - w, y - z, y - w,$ and $z - w$ are obtained by simulation as in Figure 15(a), the time domain waveform diagrams in the $x - t, y - t, z - t,$ and $w - t$ planes are shown in Figure 15(b) and the 0–1 test diagram is shown in Figure 16. From the simulated attractor phase diagrams, it can be seen that the attractor phase diagrams after dimensionality reduction are consistent with the five-dimensional chaotic system, the time-domain waveform diagrams are still irregularly varying, and the 0–1 test diagrams show Brownian motion, so the system after dimensionality reduction is still chaotic.

*6.2. Synchronized Control.* Many scholars have already applied adaptive synchronization to low-dimensional chaotic systems, while there are still few applications in high-dimensional chaotic systems, especially using heterogeneous chaotic systems

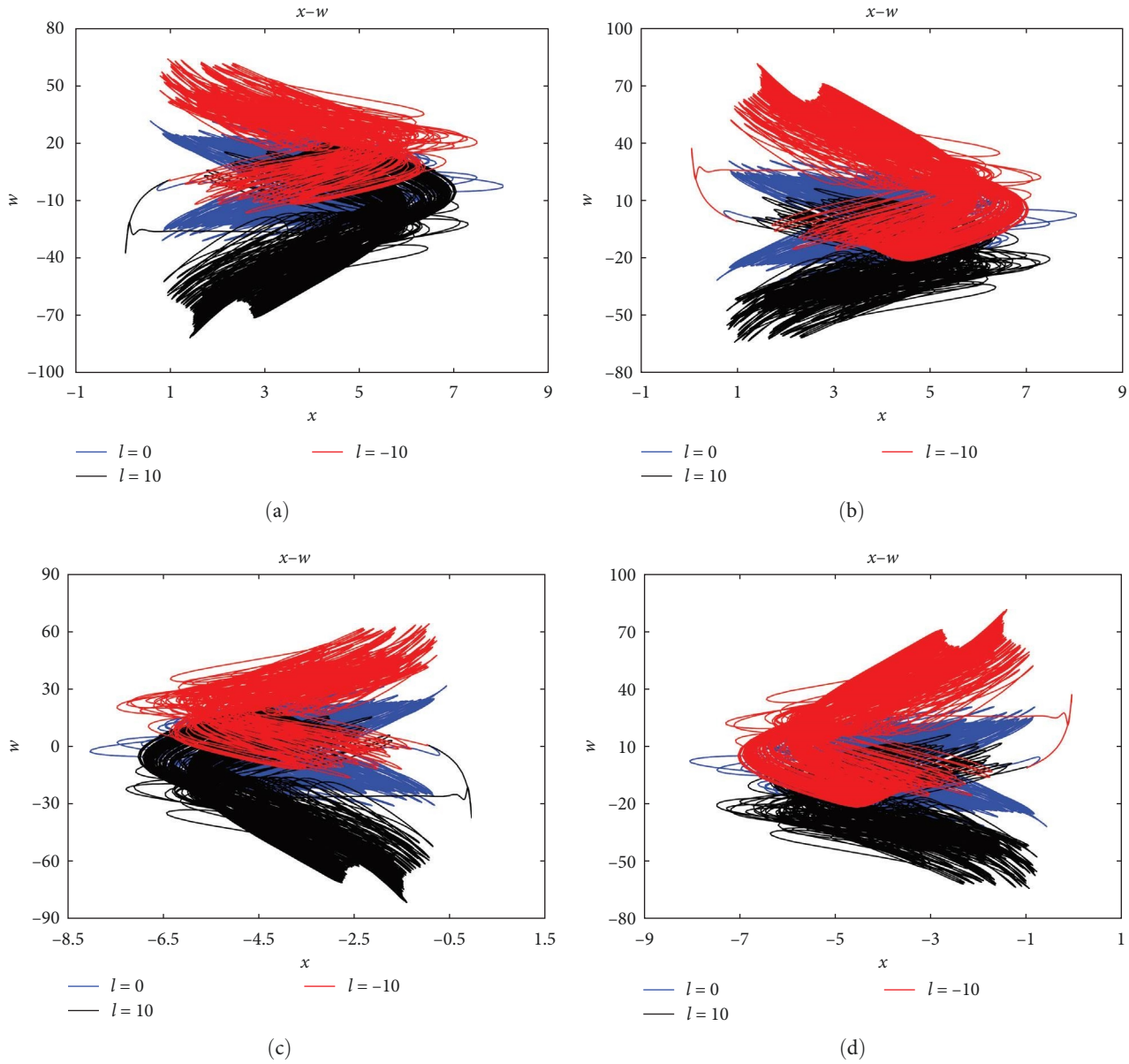


FIGURE 11: When $l = 10$, $l = 0$ and $l = -10$, attractor phase diagrams at different initial values: (a) $(1; -1; -10; 1; -10)$; (b) $(1; 1; 10; -1; 10)$; (c) $(-1; -1; -10; 1; -10)$; (d) $(-1; 1; 10; -1; 10)$.

to achieve synchronization. In this paper, the adaptive synchronization control method is adopted to achieve the synchronization of chaotic systems before and after dimensional reduction, and the specific operation steps are as follows:

Let the dimensionalized four-dimensional chaotic system (11) be used as the driving system and the five-dimensional chaotic system (3) as the response system, and for the sake of the study, the driving system is rewritten as follows:

$$\begin{cases} \dot{x}_1 = a_1 x_1 - x_1 y_1 z_1 \\ \dot{y}_1 = b_1 y_1 + {x_1}^2 z_1 - 4 w_1 \\ \dot{z}_1 = {x_1}^2 y_1 - c_1 z_1 \\ \dot{w}_1 = 40(1 + 0.01 y_1^2) y_1 - w_1 \end{cases}. \tag{12}$$

The response system is rewritten as follows:

$$\begin{cases} \dot{x}_2 = a_2 x_2 - x_2 y_2 z_2 + v_1 \\ \dot{y}_2 = b_2 y_2 + {x_2}^2 z_2 - 3 w_2 + v_2 \\ \dot{z}_2 = {x_2}^2 y_2 - c_2 z_2 + v_3 \\ \dot{w}_2 = 40(1 + 0.01 u_2^2) y_2 - w_2 + v_4 \\ \dot{u}_2 = y_2 + v_5 \end{cases}, \tag{13}$$

where $v_1, v_2, v_3, v_4$, and $v_5$ are the synchronization controllers and parameters $a_1, a_2, b_1, b_2, c_1$, and $c_2$ are unknown, to achieve synchronization between the drive and response systems in different initial states, the error between the two systems needs to be defined as follows:

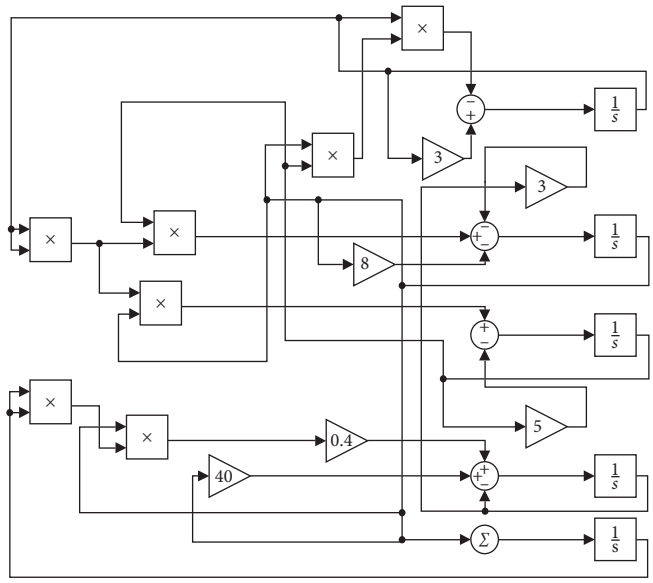


FIGURE 12: Simulink circuit diagram.

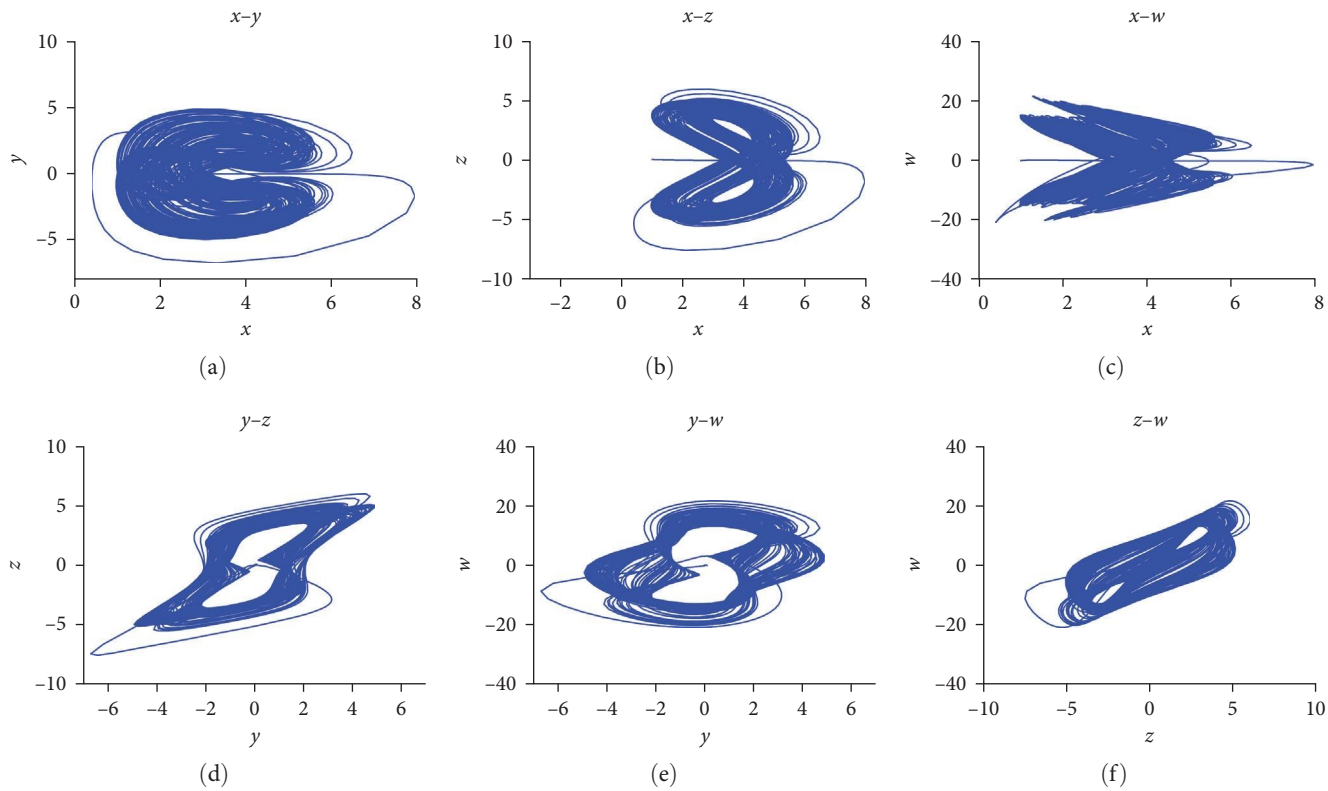


FIGURE 13: Chaotic attractor phase diagrams with parameters $a = 3$, $b = -8$, $c = 3$, $d = 5$, $e = 1$, $k = 40$, $m = 1$, and $n = 0.01$: (a) the $x$–$y$ plane; (b) the $x$–$z$ plane; (c) the $x$–$w$ plane; (d) the $y$–$z$ plane. (e) the $y$–$w$ plane; and (f) the $z$–$w$ plane.

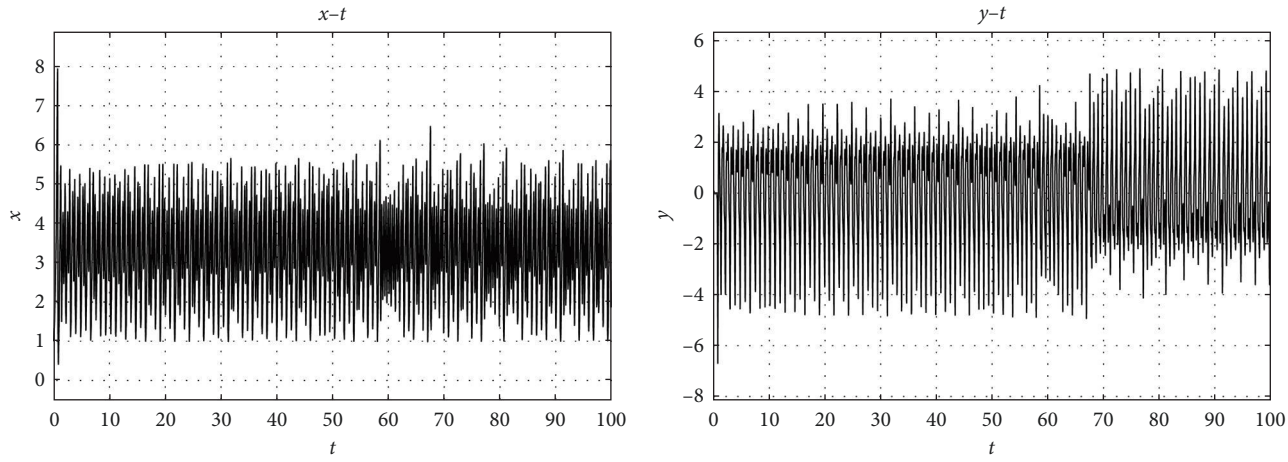


FIGURE 14: Time domain waveform with parameters $a = 3, b = -8, c = 3, d = 5, e = 1, k = 40, m = 1$, and $n = 0.01$.

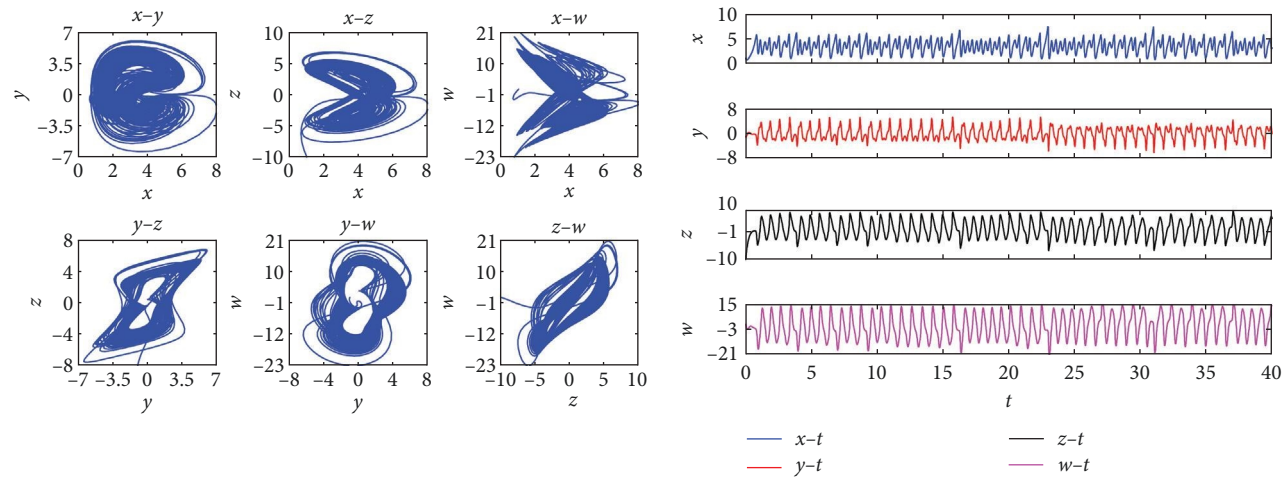


(a) (b)

FIGURE 15: Chaotic attractor phase diagrams and time domain waveforms with parameters $a = 3, b = -8, c = 4, d = 5, e = 1, k = 40, m = 1$, and $n = 0.01$: (a) attractor phase diagrams; (b) time domain waveforms.

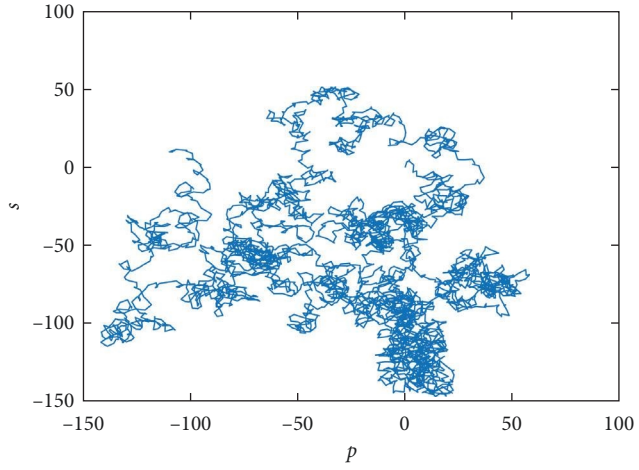


FIGURE 16: 0–1 test plot with parameters $a = 3, b = -8, c = 4, d = 5, e = 1, k = 40, m = 1$, and $n = 0.01$.

$$\begin{cases} e_1 = x_2 - x_1 \\ e_2 = y_2 - y_1 \\ e_3 = z_2 - z_1 \\ e_4 = w_2 - w_1 \\ e_5 = u_2 - u_1 \\ a = a_2 - a_1 \\ b = b_2 - b_1 \\ c = c_2 - c_1 \end{cases}. \tag{14}$$

In performing the error calculation, the four-dimensional chaotic system lacks the fifth-dimensional equation, so $e_5 = u_2 - u_1 = u_2 - 0 = y_2$, the error system equation can be obtained from the driving system (12), the response system (13), and the error variable (14) as follows:

$$\begin{cases} \dot{e}_1 = a_2x_2 - y_2x_2z_2 - a_1x_1 + y_1x_1z_1 + v_1 \\ \dot{e}_2 = b_2y_2 + x_2^2z_2 - 3w_2 - b_1y_1 - x_1^2z_1 + 4w_1 + v_2 \\ \dot{e}_3 = x_2^2y_2 - c_2z_2 - x_1^2y_1 + c_1z_1 + v_3 \\ \dot{e}_4 = 40y_2 + 0.4u_2^2y_2 - w_2 - 40y_1 - 0.4y_1^3 + w_1 + v_4 \\ \dot{e}_5 = y_2 + \mathrm{v}_5 \end{cases} . \tag{15}$$

Take the control rate as follows:

$$\begin{cases} v_1 = -y_1x_1z_1 + y_2x_2z_2 - (a_2 + 1)e_1 \\ v_2 = x_1^2z_1 - x_2^2z_2 - b_2e_2 + 3e_4 - w_1 - e_2 \\ v_3 = x_1^2y_1 - x_2^2y_2 + c_2e_3 - e_3 \\ v_4 = 40y_1 + 0.4y_1^3 - 40y_2 - 0.4u_2^2y_2 \\ \mathrm{v}_5 = -y_2 - e_5 \end{cases} . \tag{16}$$

Set the Lyapunov function to the following:

$$V = \frac{1}{2}(e_1^2 + e_2^2 + e_3^2 + e_4^2 + e_5^2 + a^2 + b^2 + c^2). \tag{17}$$

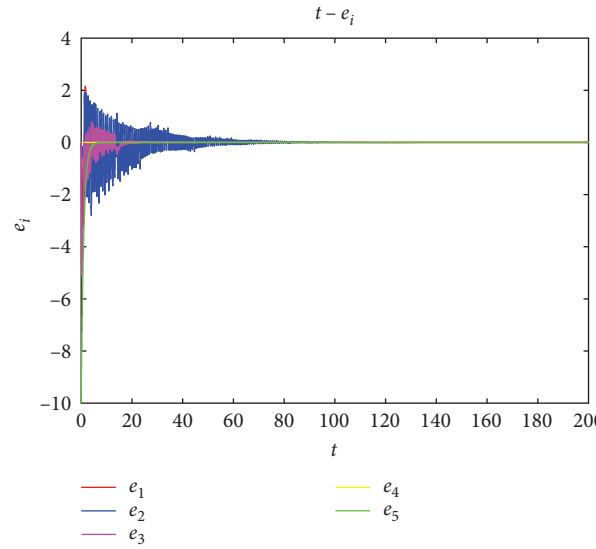


Figure 17: Synchronization error graph.

The derivative of the function $\dot{V}$ is as follows:

$$\begin{aligned} \dot{V} &= \frac{1}{2}\left(2e_1\dot{e}_1 + 2e_2\dot{e}_2 + 2e_3\dot{e}_3 + 2e_4\dot{e}_4 + 2e_5\dot{e}_5 + 2a\dot{a} + 2b\dot{b} + 2c\dot{c}\right) \\ &= \left(e_1\dot{e}_1 + e_2\dot{e}_2 + e_3\dot{e}_3 + e_4\dot{e}_4 + e_5\dot{e}_5 + a\dot{a} + b\dot{b} + c\dot{c}\right) \\ &= e_1(x_1a - e_1) + e_2(y_1b - e_2) + e_3(-z_1c - e_3) + e_4(-e_4) + e_5(-e_5) + \left(a\dot{a} + b\dot{b} + c\dot{c}\right) \end{aligned} . \tag{18}$$

The adaptive rate is taken to be as follows:

$$\begin{cases} \dot{a} = -e_1x_1 \\ \dot{b} = -e_2y_1 \\ \dot{c} = e_3z_1 \end{cases} . \tag{19}$$

Then,

$$\begin{aligned} \dot{V} &= \frac{1}{2}\left(2e_1\dot{e}_1 + 2e_2\dot{e}_2 + 2e_3\dot{e}_3 + 2e_4\dot{e}_4 + 2e_5\dot{e}_5 + 2a\dot{a} + 2b\dot{b} + 2c\dot{c}\right) \\ &= -e_1^2 - e_2^2 - e_3^2 - e_4^2 - e_5^2 \end{aligned} . \tag{20}$$

The Lyapunov function is greater than zero, and its derivative function is less than zero, so the error system is an energy decay function. As $t$ tends to infinity, $e_1$, $e_2$, $e_3$, $e_4$, and $e_5$ tends to zero, the system error tends to zero, and the drive system (11) is synchronized with the response system (3).

To verify the correctness of the synchronous controller, the synchronous controller is simulated and the initial value of the four-dimensional chaotic system is selected as $(1, -1, -10, 1)$, the initial value of the five-dimensional chaotic system is $(1, -1, -10, 1, -10)$ and the unknown parameters are $a = 3$, $b = -8$, and $c = 5$. The error results obtained from the simulation are plotted in Figure 17, and the synchronization process of the driving system and diagrams of the synchronization process between the drive system and the response system for each sequence are shown in Figure 18. It can be seen that the driving system and the responding system are synchronized at time $t = 80$, which validates the feasibility and correctness of the synchronous the feasibility and correctness of the synchronization controller are verified. It can be seen that the driving system and the response system are all synchronized at t = 80, where $x_1$ and $x_2$ are synchronized at $t = 8$, $y_1$ and $y_2$ are synchronized at $t = 80$, $z_1$ and $z_2$ are synchronized at $t = 16$, $w_1$ and $w_2$ are synchronized at $t = 0$ and $u_1$ and $u_2$ are synchronized at $t = 6$, which verifies the feasibility and correctness of this synchronized controller. Currently, there are fewer studies on the synchronous control of chaotic systems of different dimensions, especially the synchronous control of chaotic systems before and after dimensionality reduction, so considering that the time for the $y_1$ and $y_2$ error curve to converge to zero is too long, it is guessed that it may be the time delay caused by the three-dimensional nonlinear system with two positive values of the Lyapunov exponent, which itself has a higher complexity and the synchronization that is

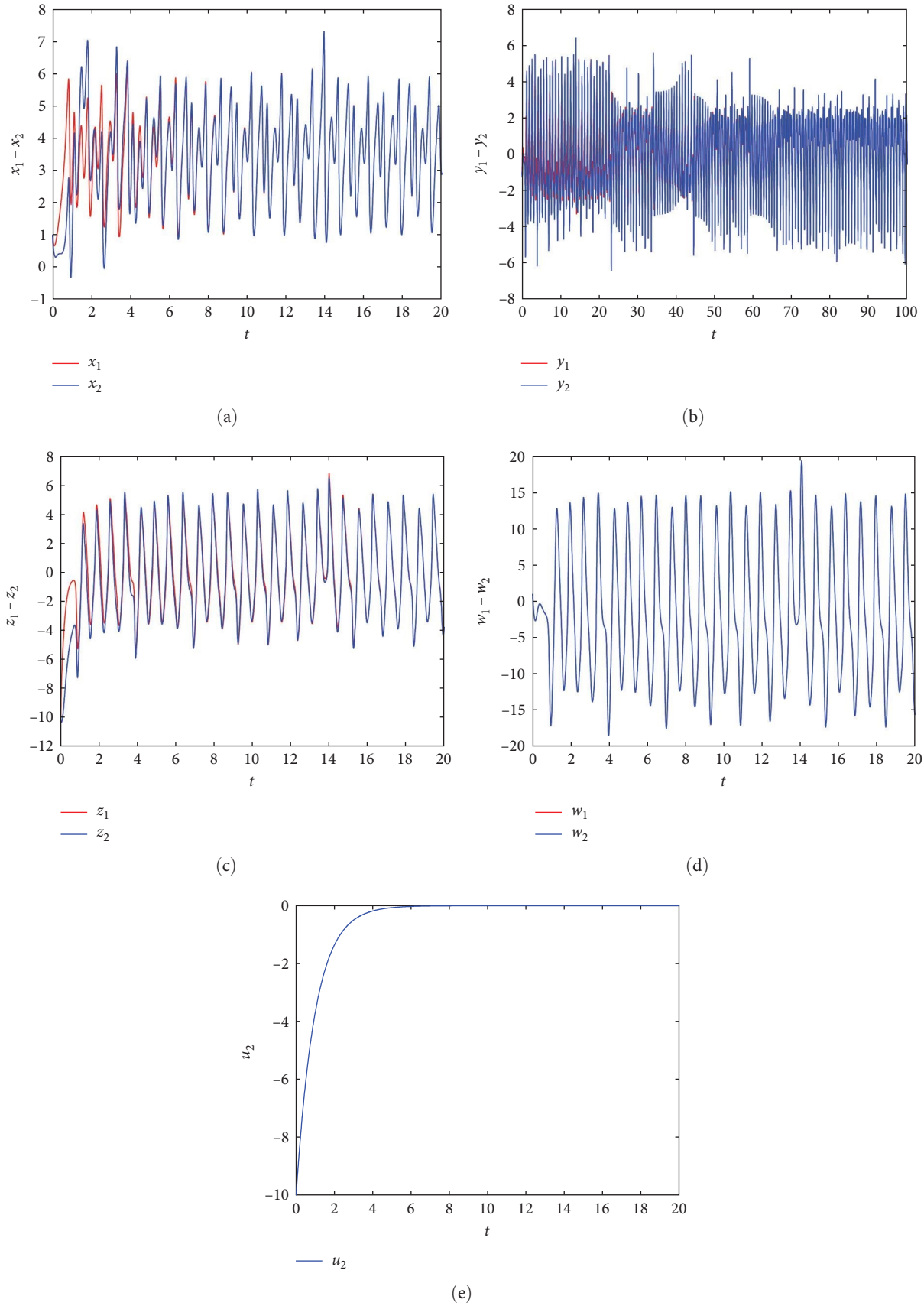


FIGURE 18: Synchronization error tracking curves for different sequences: (a) $x_1 - x_2$; (b) $y_1 - y_2$; (c) $w_1 - w_2$; (d) $z_1 - z_2$; (e) $u_2$.

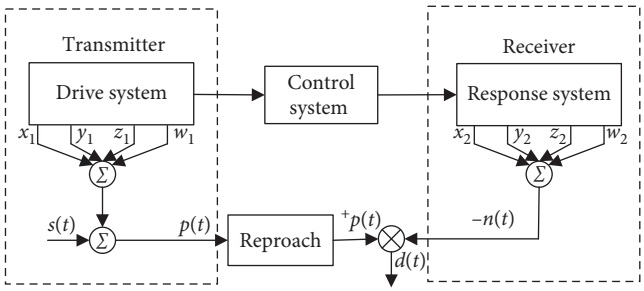


Figure 19: Schematic diagram of the communications security scheme.

Figure 20: Original image to be encrypted.

achieved by the system that will be reduced to dimensionality with itself.

*6.3. Chaos Mask Image Encryption.* The main idea of the chaotic masking technique is to superimpose the useful information signal on the signal generated by the driving system to form a modulated signal, which is transmitted using the channel, and the modulated mixed signal is demodulated using the signal generated by the response system to recover the useful information signal [32], and the communication scheme is shown in Figure 19, which is based on the fact that the driving and response systems have been realized with synchronous control. To better mask the useful information signals needed to generate more complex chaotic modulation signals, the carrier signal at the sending end and the demodulated signal at the receiving end are obtained by extracting the four corresponding state variables from the driving system and the response system, respectively and performing a simple summation. The useful information transmitted in the past are function signals; this paper proposes the use of chaotic masking technology for confidential transmission of image information, combined with theoretical analysis and experimental simulation to verify the proposed confidentiality scheme.

Carrying out experiments with high-pixel pictures will take up more resources, and the running time will be greatly lengthened, so this paper selects low-pixel pictures for

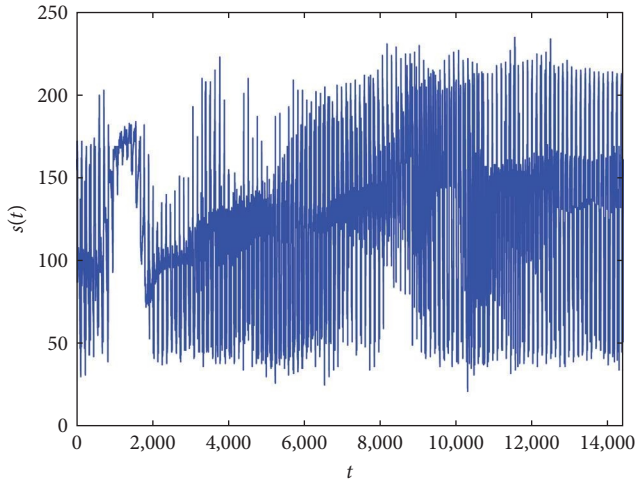


Figure 21: One-dimensional array map of the original image.

transmission and sets the information signal $s(t)$ to be transmitted as a picture with pixels of 14,400 grayscale, as shown in Figure 20. Since pictures are stored as two-dimensional arrays in the computer, they need to be modulated into one-dimensional arrays for information transfer, as shown in Figure 21.

The encryption function $p(t)$ and decryption function $d(t)$ of the chaotic masking technique used in this paper are as follows:

$$p(t) = m(1) + m(2) + m(3) + m(4) + s(t), \tag{21}$$

$$d(t) = p(t) - n(1) - n(2) - n(3) - n(4), \tag{22}$$

where $m(i)$ $(i = 1, 2, 3, 4)$ are the sequence generated by the signal of drive system $x_1, y_1, z_1$, and $w_1, p(t)$ are the encrypted aliased signal of $m(i)$ $(i = 1, 2, 3, 4)$ pair $s(t), n(i)$ $(i = 1, 2, 3, 4)$ are the chaotic synchronized sequence generated in response to the signal of system $x_2, y_2, z_2$, and $w_2$. The decrypted signals of $p(t)$ pair are $d(t)$ and $n(i)$ $(i = 1, 2, 3, 4)$.

During the synchronization test, it is obtained that the error between the driving system and the response system tends to 0 at $t = 80$ and the length of the one-dimensional array of useful information signals is 14,400. To avoid signal interference and the influence of synchronization controllers, the one-dimensional array 0–14,400 will be looped to 28,800, i.e., two repeated 0–14,400 arrays will be obtained, and the undisturbed signal can be extracted in the decryption process for the information signal reduction, i.e., the 14,400–28,800 segment array. In the experimental process, the sequences generated by the chaotic system are all four decimal places, and the useful information arrays are all integers. In MATLAB 2018a, integers can only be used in combination with the same class of integers or scalar double precision values, so it is necessary to carry out decimal operations on the useful information signal $s(t)$. The formula is as follows:

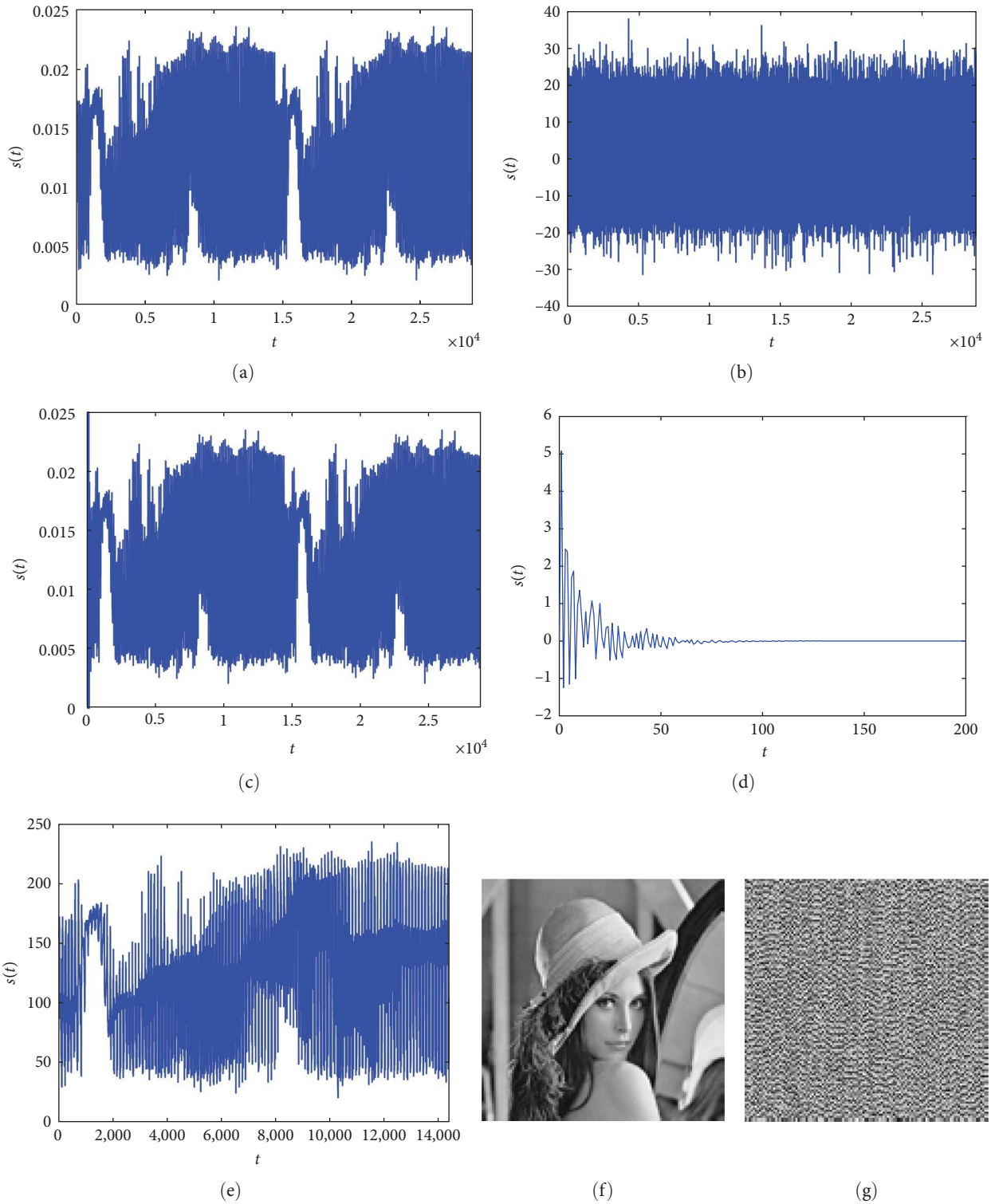


FIGURE 22: Encryption and decryption result diagrams: (a) the useful information signal $s_1(t)$; (b) the encrypted signal $p(t)$; (c) the decrypted signal $d(t)$; (d) the error diagram between useful information signal $s_1(t)$ and decrypted signal $d(t)$; (e) the 14,400–28,800 segment $d_1(t)$; (f) the encrypted image; (g) the decrypted image.

$$s_1(t) = \frac{s(t)}{10{,}000}. \tag{23}$$

The error signal between the useful information signal $s_1(t)$ and the decrypted information signal $d(t)$ is obtained as follows:

$$e(t) = s_1(t) - d(t). \tag{24}$$

To carry out the reduction of the original image, it is necessary to extract a section of one-dimensional array $d_1(t)$ and perform integer operations with the formula as follows:

$$d_2(t) = d_1(t) \cdot 10{,}000. \tag{25}$$

Based on the above encryption function, decryption function, and synchronization-related parameters, the proposed communication confidentiality scheme is simulated after fractional transformation and cyclic array operation and the obtained useful information signal $s_1(t)$ is shown in Figure 22(a); the encrypted signal $p(t)$ obtained by using the encryption function in combination with the signal generated by the driving system is shown in Figure 22(b); the decrypted signal $d(t)$ is obtained by using the decryption function in combination with the signal generated by the responding system and the decrypted signal $d(t)$ is shown in Figure 22(c); the error diagram between the useful information signal $s_1(t)$ and the decrypted signal $d(t)$ is shown in Figure 22(d); in order to restore the original image, the array $d_1(t)$ of 14,400–28,800 segments in the decrypted information signal $d(t)$ is extracted and the extracted array is subjected to integer operation by using Equation (25) and the obtained array $d_2(t)$ is shown in Figure 22(e). The 14,400–28,800 in the one-dimensional array $p(t)$ is extracted and converted into a picture, the decrypted image is shown in Figure 22(f). The one-dimensional array is converted into a picture, which is the decrypted image, as shown in Figure 22(g). From Figure 22, it can be seen that the useful information signal $s_1(t)$ is difficult to see the original signs under the mask of the encryption function and the signal $m(i)$ $(i = 1, 2, 3, 4)$ produced by the driving system and the original useful signal can be well restored under the decryption function and the signal $n(i)$ $(i = 1, 2, 3, 4)$ produced by the response system and the restored useful signal is closer to the original useful signal $s(t)$ and the restored image is closer to the original image at $t = 80$, which means that in the process of communication using the designed chaotic synchronous system before and after dimensionality reduction and based on the designed scheme can well restore the useful signal of the image and can be applied to the field of image confidentiality.

## 7. Conclusions

First, a five-dimensional memristive chaotic system with cubic nonlinear terms is constructed on a three-dimensional chaotic system. Compared with the original system, the new system has a more complex dynamical behavior, in which the system can generate identical symmetric rotational coexisting attractors in four pairs of symmetric coordinates, and the trajectories of the four coexisting attractors are independent of each other without intersecting each other, and there are also parameter-dependent periodic limit loops and transient chaotic phenomena, as well as initial-value-dependent super-multisteady-state phenomena. In studying the incremental control of the linear state variable offset of the system, it is shown experimentally that the chaotic system can be transformed between single and double poles in four pairs of symmetric coordinates. Second, the circuit construction of the cubic nonlinear memristive chaotic system using Simulink proves the correctness of the system. Finally, the important dynamics of the system are preserved, and the five-dimensional system is downgraded to a four-dimensional chaotic system, and the system is synchronized before and after the downgrading by using an adaptive synchronous control method. Using the designed linear encryption and decryption function and chaotic masking technique, combined with experimental simulation, it is to proved that the encrypted and decrypted images are basically the same and the encryption and decryption of images are completed. It is demonstrated that the proposed three-time nonlinear chaotic system combined with the chaos masking technique can be better applied in the field of communication. In this paper, there are still many imperfections in the research of encryption and decryption algorithms. Based on the proposed new system and the realization of the reduced-dimensional synchronous control, the application of chaotic masking technology to the image has been preliminarily verified, which proves that the proposed system can be applied in the field of communication, and lays a certain foundation for future encryption and decryption algorithms, and the subsequent encryption and decryption algorithms can be explored based on the chaotic system and be realized in hardware.

## Data Availability

Numerical data used to support the findings of this study are included within the article.

## Conflicts of Interest

The authors declare that there are no conflicts of interest regarding the publication of this paper.

## Acknowledgments

This work is supported by a scientific project under grant no. HKD202212, the name of the project is the Introduction of High Level Talents Research Initiation Fund Project of Heilongjiang University of Science and Technology. This work is also supported by a scientific project under grant no. 2023-KYYWF-0537, the name of the project is the High Level Cultivation Project for Basic Research Business Expenses of Provincial Undergraduate Universities in Heilongjiang Province 2023.

## References

[1] L. Xintao, G. Huaqiang, K. Shouqiang, Z. Jianliang, W. Yujing, and Z. Shi, "A new five-dimensional chaotic system and its circuit implementation," *Journal of Harbin University of Science and Technology*, vol. 20, no. 3, pp. 101–105+113, 2015.

[2] N. Lahav, I. Sendiña-Nadal, C. Hens et al., "Topological synchronization of chaotic systems," *Scientific Reports*, vol. 12, Article ID 2508, 2022.

[3] B. Feng, L. Xin, J. Maoshen, and B. Changchun, "Chaotic characterisation of audio signals," *Telecommunication Technology*, vol. 51, no. 7, 2011.

[4] W. Lei, Z. Yong, and S. Yonglu, "Dynamic analysis and numerical simulation of a class of high-dimensional chaotic models," *Practice and Understanding of Mathematics*, vol. 48, no. 12, pp. 220–226, 2018.

[5] Z. Wenjing and Z. Fuchen, "Analysis and simulation of dynamics of new nonlinear chaotic systems," *Complex Systems and Complexity Science*, vol. 20, pp. 1–9, 2023.
[6] J. C. Sprott, *Elegant Chaos: Algebraically Simple Chaotic Flows*, Singapore, World Scientific, 2010.
[7] S. Wang, S. He, A. Yousefpour, H. Jahanshahi, R. Repnik, and M. Perc, "Chaos and complexity in a fractional-order financial system with time delays," *Chaos, Solitons & Fractals*, vol. 131, Article ID 109521, 2020.
[8] V.-T. Pham, C. Volos, and L. Fortuna, "Memristor-based systems: nonlinearity, dynamics and applications," *The European Physical Journal Special Topics*, vol. 228, pp. 1903–1906, 2019.
[9] Q. Lai and Z. Chen, "Grid-scroll memristive chaotic system with application to image encryption," *Chaos, Solitons & Fractals*, vol. 170, Article ID 113341, 2023.
[10] G. D. Leutcho, L. Woodward, and F. Blanchard, "Nonlinear dynamics of a single-gap terahertz split-ring resonator under electromagnetic radiation," *Chaos: An Interdisciplinary Journal of Nonlinear Science*, vol. 33, no. 10, Article ID 103131, 2023.
[11] L. O. Chua and S. M. Kang, "Memristive devices and systems," *Proceedings of the IEEE*, vol. 64, no. 2, pp. 209–223, 1976.
[12] A. A. Rezk, A. H. Madian, A. G. Radwan, and A. M. Soliman, "Reconfigurable chaotic pseudo random number generator based on FPGA," *AEU - International Journal of Electronics and Communications*, vol. 98, pp. 174–180, 2019.
[13] M. J. Ogorzalek, *Chaos and Complexity in Nonlinear Electronic Circuits*, Vol. 22, Singapore, World Scientific, 1997.
[14] Z. Guizhong, Q. Xu, and L. Song, "Analysis and FPGA implementation of a memristive chaotic system with super-multistability," *Journal of Physics*, vol. 71, no. 24, 2022.
[15] L. Xingze and L. Junxiu, "Five-dimensional Lorentz-type memristive chaotic system and its circuit implementation," *Journal of Dalian University of Technology*, vol. 41, no. 3, pp. 220–227, 2022.
[16] L. Xiaoxia, Z. Chi, W. Xue, C. Yingzi, and X. Guizhi, "A new five-dimensional memristor super chaotic system with supermultistability," *Journal of Harbin Institute of Technology*, vol. 54, no. 3, pp. 163–170, 2022.
[17] R. Ramamoorthy, K. Rajagopal, G. D. Leutcho, O. Krejcar, H. Namazi, and I. Hussain, "Multistable dynamics and control of a new 4D memristive chaotic Sprott B system," *Chaos, Solitons & Fractals*, vol. 156, Article ID 111834, 2022.
[18] G. D. Leutcho, H. Wang, T. F. Fozin, K. Sun, Z. T. Njitacke, and J. Kengne, "Dynamics of a new multistable 4D hyperchaotic Lorenz system and its applications," *International Journal of Bifurcation and Chaos*, vol. 32, no. 1, Article ID 2250001, 2022.
[19] Q. Lai, Z. Wan, and P. D. K. Kuate, "Generating grid multi-scroll attractors in memristive neural networks," *IEEE Transactions on Circuits and Systems I: Regular Papers*, vol. 70, no. 3, pp. 1324–1336, 2023.
[20] Q. Lai and Z. Chen, "Dynamical analysis and finite-time synchronization of grid-scroll memristive chaotic system without equilibrium," *Chaos, Solitons & Fractals*, vol. 176, Article ID 114118, 2023.
[21] Q. Lai, L. Yang, and G. Chen, "Design and performance analysis of discrete memristive hyperchaotic systems with stuffed cube attractors and ultraboosting behaviors," *IEEE Transactions on Industrial Electronics*, pp. 1–10, 2023.
[22] Q. Xu, Q. Da, S. Zhi-Peng, Z. Gui-Zhong, and L. Song, "Dynamical analysis and FPGA implementation of a fourth-order chaotic system with coexisting attractors," *Acta Physica Sinica*, vol. 72, no. 19, Article ID 190502, 2023.
[23] I. Birs, C. Muresan, I. Nascu, and C. Ionescu, "A survey of recent advances in fractional order control for time delay systems," *IEEE Access*, vol. 7, pp. 30951–30965, 2019.
[24] A. T. Azar, S. Vaidyanathan, and A. Ouannas, *Fractional Order Control and Synchronization of Chaotic Systems*, Vol. 688, Springer, Berlin/Heidelberg, Germany, 2017.
[25] B. Yan, F. Parastesh, S. He, K. Rajagopal, S. Jafari, and M. Perc, "Interlayer and intralayer synchronization in multiplex fractional-order neuronal networks," *Fractals*, vol. 30, no. 10, Article ID 2240194, 2022.
[26] H. Jahanshahi, M. Jafarzadeh, N. N. Sari, V.-T. Pham, V. V. Huynh, and X. Q. Nguyen, "Robot motion planning in an unknown environment with danger space," *Electronics*, vol. 8, no. 2, Article ID 201, 2019.
[27] N. Najafizadeh Sari, H. Jahanshahi, and M. Fakoor, "Adaptive fuzzy PID control strategy for spacecraft attitude control," *International Journal of Fuzzy Systems*, vol. 21, pp. 769–781, 2019.
[28] S. Emiroglu, Y. Uyaroglu, and T. E. Gümüş, "Recursive backstepping control of ferroresonant chaotic oscillations consisting between grading capacitor with nonlinear inductance of voltage transformer," *The European Physical Journal Special Topics*, vol. 230, pp. 1829–1837, 2021.
[29] S. Emiroglu, A. Akgül, Y. Adıyaman, T. E. Gümüş, Y. Uyaroglu, and M. A. Yalçın, "A new hyperchaotic system from T chaotic system: dynamical analysis, circuit implementation, control and synchronization," *Circuit World*, vol. 48, no. 2, pp. 265–277, 2022.
[30] P. Alexander, S. Emiroğlu, S. Kanagaraj, A. Akgul, and K. Rajagopal, "Infinite coexisting attractors in an autonomous hyperchaotic megastable oscillator and linear quadratic regulator-based control and synchronization," *The European Physical Journal B*, vol. 96, Article ID 12, 2023.
[31] Z. Chi, *Research on Multi-Stationary Chaotic Systems and their Synchronous Control*, Hebei University of Technology, 2022.
[32] L. Liu, *Design and FPGA implementation of a Five-Dimensional Super Chaotic System Based on Memristor*, Changsha University of Science and Technology, 2023.
[33] W. Shi, *Research and Synchronous Application Based on a New Three-Dimensional Chaotic System*, Northwest Normal University, 2023.
[34] K. Rajagopal, H. Jahanshahi, M. Varan et al., "A hyperchaotic memristor oscillator with fuzzy based chaos control and LQR based chaos synchronization," *AEU - International Journal of Electronics and Communications*, vol. 94, pp. 55–68, 2018.
[35] A. Yousefpour and H. Jahanshahi, "Fast disturbance-observer-based robust integral terminal sliding mode control of a hyperchaotic memristor oscillator," *The European Physical Journal Special Topics*, vol. 228, pp. 2247–2268, 2019.
[36] A. Yousefpour, H. Jahanshahi, J. M. Munoz-Pacheco, S. Bekiros, and Z. Wei, "A fractional-order hyper-chaotic economic system with transient chaos," *Chaos, Solitons & Fractals*, vol. 130, Article ID 109400, 2020.
[37] H. Jahanshahi, A. Yousefpour, Z. Wei, R. Alcaraz, and S. Bekiros, "A financial hyperchaotic system with coexisting attractors: dynamic investigation, entropy analysis, control and synchronization," *Chaos, Solitons & Fractals*, vol. 126, pp. 66–77, 2019.
[38] B. Bocheng, H. Wen, X. Jian ping, L. Zhong, and Z. Ling, "Analysis and implementation of memristor chaotic circuits," *Journal of Physics*, vol. 60, no. 12, pp. 63–70, 2011.
[39] W. Liu and G. Chen, "A new chaotic system and its generation," *International Journal of Bifurcation and Chaos*, vol. 13, no. 1, pp. 261–267, 2003.

[40] W. Liu and G. Chen, "Can a three-dimensional smooth autonomous quadratic chaotic system generate a single four-scroll attractor?" *International Journal of Bifurcation and Chaos*, vol. 14, no. 4, pp. 1395–1403, 2004.

[41] F. Yi-Gang, "Research on high-order hidden chaotic systems," *China New Technology and New Products*, vol. 11, pp. 55–57, 2022.

[42] C. Dumitrescu, "Contributions to modeling the behavior of chaotic systems with applicability in economic systems," *Internal Auditing and Risk Management*, vol. 56, no. 4, pp. 98–107, 2019.

[43] L. M. Pecora and T. L. Carroll, "Synchronization of chaotic systems," *Chaos: An Interdisciplinary Journal of Nonlinear Science*, vol. 25, no. 9, Article ID 097611, 2015.

[44] Z. Zhaoteng, *Research on New Constant LE Spectral Chaos and Hidden Attractor Memristor Super Chaotic System*, Hunan Normal University, 2021.